Reliability Engineering and System Safety 267 (2026) 111856

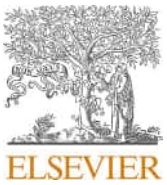

Contents lists available at ScienceDirect

Reliability Engineering and System Safety

journal homepage: www.elsevier.com/locate/ress

Imprecise model of thunderstorm wind speed and uncertainty propagation on the maximum dynamic response

Luca Roncallo [a], Alba Sofi [b,*], Giuseppe Muscolino [c], Federica Tubino [a]

[a] Department of Civil, Chemical and Environmental Engineering, University of Genoa, Genoa, Italy
[b] Department of Architecture and Design, University "Mediterranea" of Reggio Calabria, Reggio Calabria, Italy
[c] Department of Engineering, University of Messina, Messina, Italy

ARTICLE INFO

Keywords:
Interval analysis
Uncertainty propagation
Thunderstorm downburst
Non-stationary dynamic response

ABSTRACT

The wind velocity field associated with thunderstorm downbursts can be modelled as a uniformly modulated nonstationary random process, characterized by an Evolutionary Power Spectral Density function. The parameters characterizing the evolutionary model vary significantly from one thunderstorm to another. Due to the limited data availability, the interval model appears to be a suitable approach to represent the uncertainty of such parameters. In this paper, by leveraging available thunderstorm data and a literature-based model for the vertical profile of mean velocity, appropriate bounds for the key loading parameters are established, and an interval model for the thunderstorm wind speed is introduced. Employing a closed-form solution for the gust response factor and based on the introduced interval model of the thunderstorm wind speed, this study investigates the propagation of uncertainties on the thunderstorm gust response factor and the maximum dynamic response for slender vertical structures using the Improved Interval Analysis. Results indicate that, for the structural cases analyzed, uncertainties in thunderstorm parameters exert a more significant influence on the thunderstorm gust response factor and maximum response than those in the structural parameters.

1. Introduction

Wind and earthquakes constitute the main natural hazards that strike the built environment, causing damages and losses in our societies. Focusing on the wind climate, the occurrence of extra-tropical cyclones and thunderstorm downbursts characterises several locations worldwide [1,2]. Considering time intervals between 10 min and 1 h, the wind velocity field associated with synoptic events such as extra-tropical cyclones is modelled as the superimposition of a mean wind velocity that is constant in time and varies with the height according to a logarithmic profile, and the atmospheric turbulence, modelled as a Gaussian stationary random process characterized by its Power Spectral Density (PSD) function [3]. Thunderstorm downbursts are mesoscale phenomena that differ from extra-tropical cyclones in multiple ways, from their genesis in the atmosphere to their wind structure [4]. Specifically, the wind field associated with a thunderstorm outflow shows a nose-shaped mean wind speed profile and nonstationary behaviour over short time intervals [5]. Because of these substantial differences with extra-tropical cyclones, several models have been introduced for representing the nose-shaped mean wind speed profile (e.g. [6–8]), among which the model by [8,9] is the most widely adopted in the literature. Furthermore, considering the wind speed at a point in space, the velocity is commonly represented as the superimposition of a slowly-varying mean component and a nonstationary fluctuation, modelled as a uniformly modulated nonstationary random process [10,11]. Based on these assumptions, an Evolutionary Power Spectral Density (EPSD) model of thunderstorm outflows consistent with full-scale wind speed records was developed by [12], aiming to encapsulate the essential features of the nonstationary turbulent fluctuations.

Focusing on the wind-excited response of structures, it is established practice with stationary winds to convert the wind speed into aerodynamic loading under the assumption of small turbulence, neglecting the quadratic term of the fluctuations. Consequently, the aerodynamic loading follows a Gaussian distribution. For structures exhibiting linear elastic behaviour, their response is also represented as a Gaussian stationary random process. This scheme is commonly referred to as Davenport wind loading chain [13]. Moreover, the distribution of the maximum response is derived under the assumption that up-crossings of a sufficiently high threshold are rare and independent events. Since the distribution of the maximum dynamic response is narrow, it is

* Corresponding author.
E-mail address: alba.sofi@unirc.it (A. Sofi).

https://doi.org/10.1016/j.ress.2025.111856
Received 27 March 2025; Received in revised form 29 September 2025; Accepted 26 October 2025
Available online 28 October 2025

commonly represented by its mean value. This approach facilitated the development of the gust response factor technique, widely adopted for engineering calculations and code applications. Indeed, nowadays, codes and standards provide suitable tools for engineers to deal with the wind-resistant structural design related to extra-tropical cyclones [14–16], based on the gust-factor technique [13].

Because of the nonstationary nature of the thunderstorm wind speed, the dynamic response of structures to thunderstorm downbursts is also a nonstationary random process, characterized by an EPSD function that can be regarded as the output of a generalized Davenport wind loading chain [17]. The mean value of the maximum dynamic response should be estimated from its probability density function defined on the basis of the up-crossing theory of nonstationary processes, taking into account the variation in time of the mean part of the response and the standard deviation [18–20]. However, this approach is not suitable for rapid engineering calculations and is not appropriate for integration into a code design framework. Following the same philosophy of the gust factor technique for stationary winds, the Thunderstorm Gust Response Factor (TGRF) technique has been recently developed, which accounts for the transient dynamic response induced by the nonstationary wind loading described by the EPSD model [21]. Successively, a closed-form solution was developed by [22] to improve the handiness of the approach, facilitating the estimate of the maximum response of structures to thunderstorm outflows [23].

Despite the potential of the TGRF technique, its usage requires a reliable characterization of the thunderstorm wind speed parameters that shape the EPSD, which are usually difficult to define due to either the lack of thunderstorm data or the great variability of the phenomenon. Indeed, the analysis of a wide set of thunderstorm recordings [24,25] has shown a large variability of the thunderstorm parameters from one recording to another. The quantification of the uncertainties affecting these parameters is of potential interest for defining suitable safety factors for structures subjected to thunderstorm wind loading. In the literature, based on their source, uncertainties are usually classified as aleatory or epistemic [26,27]. Aleatory uncertainties are properly modeled using probabilistic methods, which require a large amount of data to define the relevant probability density functions. It is widely recognized that the reliability of probabilistic approaches is not guaranteed when limited data are available [28]. When information on various sources of uncertainty is incomplete or fragmentary, the use of non-probabilistic approaches [29–32] is more appropriate for retrieving reliable predictions of the safety level [33]. The awareness of possible limitations of traditional probabilistic methods [30] has motivated the use of non-probabilistic uncertainty descriptions, such as the interval model [34,35], convex models [36] or fuzzy-sets [37], in conjunction with classical methods for structural reliability analysis and reliability-based optimization (see e.g. [38–44]). Reliability analysis under hybrid or mixed uncertainties, i.e. involving both random and interval variables, has also attracted significant research interest (see, e.g. [45–49]). Furthermore, efficient approaches have been developed to perform reliability analysis in the presence of uncertain parameters described by means of imprecise probabilities, which arise from epistemic uncertainty in the definition of the relevant hyper-parameters (see e.g., [50–52]). Recently, some studies have been devoted to estimating the PSD and EPSD function of stochastic excitation processes by considering epistemic uncertainties in the data records and evaluating the associated structural response [53–58]. To the best of the authors' knowledge, attention has been focused on seismic excitation, while the influence of epistemic uncertainties on the characterization of wind velocity has not yet been addressed.

In this paper, epistemic uncertainties affecting the relevant EPSD of the thunderstorm wind velocity are described as interval variables using the Improved Interval Analysis via Extra Unitary Interval (IIA via EUI) [59]. To characterize such intervals, the time histories of many recorded thunderstorms are analysed. Chauvenet's criterion [60,61] is applied to discard outliers from the set of wind velocity time histories. As a final outcome of the statistical analysis of the selected thunderstorms, the ranges of variability of the main parameters of the EPSD function are determined. Therefore, an imprecise model is introduced for the EPSD function representative of wind velocity time histories recorded during thunderstorms, as a function of interval parameters [34,35].

The dynamic analysis of structural systems subjected to imprecise stochastic excitation is a challenging task since it involves the propagation of hybrid uncertainty, i.e., interval and random. Assuming that the effects of aleatoric and epistemic uncertainty are kept separated [62], hybrid uncertainty can be propagated by solving a double-loop problem. This approach demands significant computational effort and quickly becomes unfeasible for real-world engineering applications.

Starting from the imprecise model of the thunderstorm wind speed, the present study introduces an interval model of the thunderstorm gust factor and the maximum dynamic response, including also the uncertainties associated with the main mechanical and dynamical parameters of the structure. The availability of closed-form expressions for the gust response factor and maximum dynamic response allows performing the stochastic analysis of structures subjected to imprecise thunderstorm wind loading by decoupling the propagation of interval and random uncertainties. Furthermore, sensitivities of the maximum dynamic response of structures to the interval loading and structural parameters can be derived by direct differentiation, and analytical expressions of its upper and lower bounds can be obtained. Thus, the propagation of the uncertainties in the thunderstorm parameters on the maximum dynamic response is studied. Two real case studies are selected: a lighting pole and a telecommunications tower. In this framework, the bounds of the TGRF and maximum response are derived analytically by varying the degree of uncertainty of parameters, carrying out separate analyses for the wind loading and structural uncertainties.

The paper is articulated as follows: Section 2 introduces the analytical framework of the thunderstorm wind speed modelling and related maximum dynamic response characterization by means of the TGRF; Section 3 presents the model of the imprecise thunderstorm wind speed and response based on the Improved Interval Analysis; Section 4 outlines the bounds of the thunderstorm wind speed model and response sensitivity based on the available time histories; Section 5 presents numerical results for two structural case studies; finally, Section 6 outlines the conclusions and future outcomes of this research.

2. Definition of the thunderstorm excitation and response

This section introduces the analytical framework concerning the thunderstorm wind speed modelling (Section 2.1) and the characterization of the Thunderstorm Gust Response Factor (TGRF) and maximum dynamic response (Section 2.2).

2.1. Thunderstorm wind speed

Let us consider the thunderstorm wind speed $v(z,t)$ along the vertical coordinate z, where $z = 0$ m at the ground level. It can be represented as the sum of a slowly-varying mean $v_m(z,t)$ and a nonstationary turbulent fluctuation component $v'(z,t)$ as follows [23,63]

$$v(z,t) = v_m(z,t) + v'(z,t) \tag{1}$$

with t being the time. The slowly-varying mean wind speed can be expressed as follows:

$$v_m(z,t) = v_{\max}\alpha(z)\gamma(t). \tag{2}$$

In Eq. (2), $v_{\max}$ is the maximum value of the slowly-varying mean wind speed at the reference height h, $\gamma(t)$ the modulating function of the mean wind speed, and $\alpha(z)$ its vertical profile. The modulating function and vertical profile are defined according to models from the literature and read [8,25]:

$$\gamma(t) = \begin{cases} \dfrac{1-\gamma*}{2}\left[\cos\left(\dfrac{2\pi t}{T}\right)+1\right]+\gamma*, & |t| < \dfrac{T}{2} \\ \gamma*, & |t| \geq \dfrac{T}{2} \end{cases} \tag{3}$$

$$\alpha(z) = \left(\frac{z}{h}\right)^{1/6}\left(\frac{1-\mathrm{erf}[0.1167z/z_m]}{1-\mathrm{erf}[0.1167h/z_m]}\right) \tag{4}$$

where $\gamma*$ is a measure of the intensity of the background mean wind speed, $T$the duration of the intense phase of the outflow, and z_m is the height of the tip of the nose-shaped vertical profile. Fig. 1a and b show, respectively, the vertical profile and the modulating function of the mean wind speed and the associated parameters.

The nonstationary turbulent fluctuation $v'(z,t)$ is regarded as a uniformly modulated [12] process and its Evolutionary Power Spectral Density (EPSD) at a point in space reads:

$$S_{v'}(z,t,n) = v_{\max}^2 I_v^2 \gamma^2(t)\alpha^2(z)\theta^2(z)S_{\tilde{v}'}(z,n) \tag{5}$$

where I_v is the average value of the turbulence intensity at the reference height h (assumed constant over 10 min), $\theta(z)$ is the vertical profile of the turbulence intensity, and $S_{\tilde{v}'}(z,n)$ the Power Spectral Density (PSD) of the reduced turbulent fluctuation $\tilde{v}'(z,t)$ [64]. Concerning the vertical profile of the turbulence intensity, a widely accepted model is not available in the literature. In this paper, the model $\theta(z) = 1/\alpha(z)$ proposed in [23] is adopted:

$$\theta(z) = \frac{1-\mathrm{erf}(0.1167h/z_m)}{\left(\frac{z}{h}\right)^{1/6}[1-\mathrm{erf}(0.1167z/z_m)]}. \tag{6}$$

Employing the model by [65], the PSD of the reduced turbulent fluctuations is given by:

$$S_{\tilde{v}'}(z,n) = \frac{d_v L_v/[v_{\max}\alpha(z)]}{\{1+1.5nL_v/[v_{\max}\alpha(z)]\}^{5/3}} \tag{7}$$

where L_v is the integral length scale of the turbulence and d_v=6.868. It is worth noting that the integral length scale of turbulence varies with the height for synoptic winds. The variation of the integral length scale with height during thunderstorm outflows is poorly documented. Zhang et al. [24] reported values of the integral length scale extracted from anemometric measurements of different thunderstorm events at fixed heights in different locations, which are not suitable for deducing a profile. Romanic [66] analysed a nocturnal thunderstorm, reporting an increasing trend with the height of the length scale parameter; however, an expression for the vertical profile of the integral length scale of turbulence was not proposed. Therefore, in this study, the variation of L_v with the height is neglected. As an example, Fig. 2a and b plot, respectively, the vertical profiles of the turbulence intensity and the PSD model of the turbulence.

The definition of the EPSD in Eq. (5) is fundamental for the derivation and study of the dynamic response to thunderstorm downbursts and its maximum value. Therefore, in view of the great variability of the thunderstorm events [25], it is of utmost importance to properly define the parameters of the relevant EPSD and the associated uncertainties.

2.2. Thunderstorm gust response factor and maximum dynamic response

Let us consider a slender vertical structure, schematized as a continuous linear elastic cantilever beam characterized by height H, width $b(z)$ and drag coefficient $c_D(z)$, z being the vertical coordinate. The structure is subjected to the wind loading produced by a thunderstorm outflow outlined in Section 2.1. It is assumed that the dynamic response is dominated by its first mode of vibration with mode shape $\psi_1(z)$, first natural frequency n_1, modal mass m_1, and damping ξ. Adopting the TGRF technique, the maximum horizontal displacement $q_{\max}$ experienced by the structure at the top $z = H$ is estimated as follows [23,63]:

$$q_{\max} = G_q q_{\mathrm{m}} \tag{8}$$

where q_{m} is the maximum of the mean part of the response and G_q denotes the TGRF. They read, respectively:

$$q_{\mathrm{m}} = \frac{\rho v_m^2}{2m_1(2\pi n_1)^2}\int_0^H \alpha^2(z)b(z)c_D(z)\psi_1(z)dz \tag{9}$$

$$G_q = 1 + 2\mathscr{C}I_v g_q(\nu_q T_{eq})\sqrt{B^2+R^2}. \tag{10}$$

In Eqs. (9) and (10), ρ is the air density, g_q is the Davenport peak factor, ν_q the expected frequency, B and R are, respectively, the background and resonance factors [13,15], while $\mathscr{C}$ and T_{eq} denote the equivalent parameters. These parameters can be derived in closed form, and their formulation is reported in Appendix 1.

3. Proposed model of the imprecise thunderstorm wind speed and response

In view of the uncertainties associated with the thunderstorm wind speed parameters, their propagation on the results in terms of dynamic response needs to be investigated. In this framework, it is common practice to define the probability density function of uncertain parameters [67,68] following probabilistic approaches that require an extensive amount of data, often unavailable, especially when it comes to

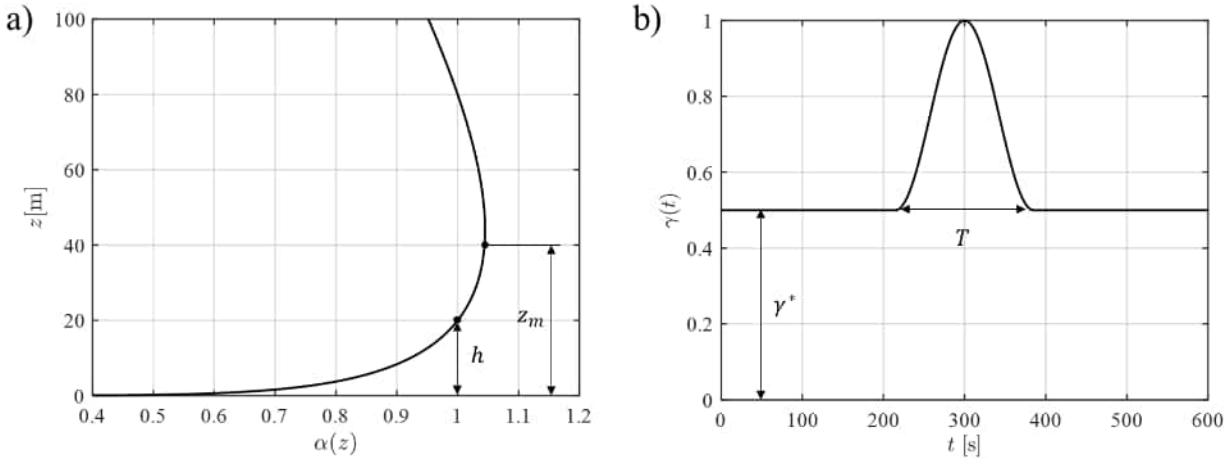

Fig. 1. (a) Vertical profile $\alpha(z)$ and (b) modulating function $\gamma(t)$ of the mean wind speed.

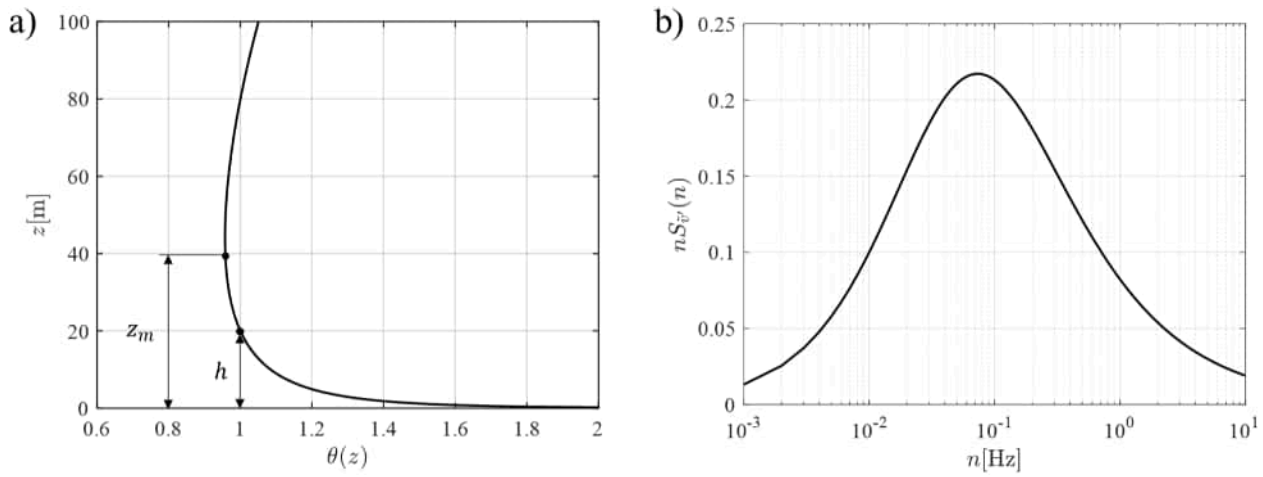

Fig. 2. (a) Vertical profile of the turbulence intensity $\theta(z)$ and (b) PSD model of the turbulence $S_{\dot{v}}(z)$.

thunderstorms. In these circumstances, modelling a parameter as a probabilistic quantity is not advisable. Therefore, in this study, the aforementioned uncertainties affecting the EPSD of the thunderstorm wind speed are addressed using interval analysis [34,35], which, together with convex models [36] or fuzzy-sets [37], is a commonly used non-probabilistic approach for addressing uncertainty when few data are available.

In this section, the interval model of the thunderstorm wind speed is first introduced (Section 3.1), then the associated interval maximum dynamic response is presented (Section 3.2).

3.1. Interval model of thunderstorm wind speed

According to the interval model, the generic parameter characterizing the EPSD function in Eq. (5) is described as an interval variable, defined by its lower bound (LB), upper bound (UB), or by the midpoint and deviation amplitude [34,35]. No information on the probability of occurrence of values over the interval is requested. One of the main drawbacks of the interval model is the overestimation of the interval solution range, which may lead to overly conservative results for engineering purposes [35]. Overestimation is caused by the so-called *dependency phenomenon,* which occurs due to the inability of *Classical Interval Analysis* [35] to recognize multiple occurrences of the same interval variable in an expression. To limit conservatism, in the present study, the Improved Interval Analysis (IIA) via Extra Unitary Interval (EUI) [59] is adopted. Accordingly, the k-th interval variable is defined as:

$$x_k^I = \left[\underline{x}_k, \overline{x}_k\right] = x_{k,0} + \Delta x_k \widehat{e}_k^I = x_{k,0}\left(1 + \Delta\chi_k \widehat{e}_k^I\right) \tag{11}$$

where $\underline{x}_k$ and $\overline{x}_k$ are, respectively, the LB and UB of the interval variable x_k^I, $\widehat{e}_k^I = [-1, +1]$ is a particular unitary interval called EUI [59], $x_{k,0}$ is the nominal value or midpoint, Δx_k the deviation amplitude, and $\Delta\chi_k$ the normalized deviation amplitude. They read, respectively:

$$x_{k,0} = \frac{\overline{x}_k + \underline{x}_k}{2} \tag{12}$$

$$\Delta x_k = \frac{\overline{x}_k - \underline{x}_k}{2} \tag{13}$$

$$\Delta\chi_k = \frac{\Delta x_k}{x_{k,0}} = \frac{\overline{x}_k - \underline{x}_k}{2x_{k,0}}. \tag{14}$$

It is worth noticing that $\Delta x_k > 0$ and $\Delta\chi_k \in [0, 1]$. Furthermore, the subscript k in $\widehat{e}_k^I$ means that the EUI is associated with the k −th interval variable. This feature enables one to keep track of dependencies among interval variables throughout calculations, thereby reducing overestimation.

Consider now a generic interval-valued function f of the interval variables x_i^I, with $(i = 1, \ldots, N_i)$, and of non-interval quantities u_l, with $(l = 1, \ldots, N_l)$, it can be equivalently denoted as:

$$f^I(u_1, u_2, \ldots x_1, x_2, \ldots) \equiv f\left(u_1, u_2, \ldots x_1^I, x_2^I, \ldots\right). \tag{15}$$

The EPSD in Eq. (5) depends on five parameters – i.e. $\gamma*$, T, I_v, L_v, z_m– which are treated as interval variables in the framework of the IIA via EUI, i.e.:

$$\gamma^{*I} = \left[\underline{\gamma}^*, \overline{\gamma}^*\right] = \gamma_0^* + \Delta\gamma^* \widehat{e}_1^I = \gamma_0^*\left(1 + \Delta\chi_{\gamma^*} \widehat{e}_1^I\right) \tag{16}$$

$$T^I = \left[\underline{T}, \overline{T}\right] = T_0 + \Delta T \widehat{e}_2^I = T_0\left(1 + \Delta\chi_T \widehat{e}_2^I\right) \tag{17}$$

$$I_v^I = \left[\underline{I}_v, \overline{I}_v\right] = I_{v,0} + \Delta I_v \widehat{e}_3^I = I_{v,0}\left(1 + \Delta\chi_{I_v} \widehat{e}_3^I\right) \tag{18}$$

$$L_v^I = \left[\underline{L}_v, \overline{L}_v\right] = L_{v,0} + \Delta L_v \widehat{e}_4^I = L_{v,0}\left(1 + \Delta\chi_{L_v} \widehat{e}_4^I\right) \tag{19}$$

$$z_m^I = \left[\underline{z}_m, \overline{z}_m\right] = z_{m,0} + \Delta z_m \widehat{e}_5^I = z_{m,0}\left(1 + \Delta\chi_{z_m} \widehat{e}_5^I\right). \tag{20}$$

These variables, associated with the wind speed (loading L) uncertainties, are collected into the following interval vector:

$$\mathbf{x}_L^I = \left\{\gamma^{*I}, T^I, I_v^I, L_v^I, z_m^I\right\}^{\mathrm{T}}. \tag{21}$$

It is worth remarking that the interval variables in Eqs. (16)–(20) are independent and therefore are defined in terms of different EUIs $\widehat{e}_k^I$ $(k = 1, 2, \ldots, 5)$. Based on Eqs (16)–(20), the EPSD function of the thunderstorm wind speed in Eq. (5) is consistently modelled as an interval function. Specifically, considering Eq. (15) and the interval parameters in Eqs. (16)–(20), the EPSD function in Eq. (5) can be written as

$$S_{\dot{v}}^I(z, t, n) \equiv S_{\dot{v}}\left(z, t, n; \mathbf{x}_L^I\right) \equiv v_{\max}^2 \left[I_v^I\right]^2 \left[\gamma^I(t)\right]^2 \left[\alpha^I(z)\right]^2 \left[\theta^I(z)\right]^2 S_{\tilde{v}}^I(z, n) \tag{22}$$

where the functions $\gamma^I(t)$, $\alpha^I(z)$, $\theta^I(z)$ and $S_{\tilde{v}}^I(z, n)$ are now interval functions of the interval parameters.

It should be noted that the maximum mean wind speed $v_{\max}$ is modelled as deterministic since it is assumed that it can be determined as a function of the design return period based on statistical analyses.

3.2. Interval maximum dynamic response

In view of the dependence of the maximum dynamic response on the interval EPSD model in Eq. (22), it follows that both the TGRF and maximum response possess interval characteristics. Moreover, the structural and aerodynamic parameters also exhibit a certain level of uncertainty. Such parameters include the drag coefficient, damping ratio, modal mass and fundamental frequency.

Specifically, the uncertainty in the drag coefficient when dealing with thunderstorm-induced loading derives from the transient nature of the wind flow and its abrupt change of direction. However, the drag coefficient depends on the shape of the cross-section and is independent of the angle of attack for circular cross-sections. Limiting our interest to circular cross-sections, the drag coefficient is assumed as deterministic in this study.

Focusing on the modal mass, its derivation is usually carried out with a significant degree of accuracy, and no particular uncertainty is involved.

The uncertainties affecting the modal frequency and damping ratio are worth considering [68,69]. Therefore, these two quantities are treated as interval variables, denoted hereafter as n_1^I and ξ^I. The vector of interval variables associated with the structural uncertainties (S) is expressed as:

$$\mathbf{x}_S^I = \{n_1^I, \xi^I\}^{\mathrm{T}} \tag{23}$$

where

$$n_1^I = \left[\underline{n}_1, \overline{n}_1\right] = n_{1,0} + \Delta n_1 \widehat{e}_6^I = n_{1,0}\left(1 + \Delta\chi_{n_1}\widehat{e}_6^I\right) \tag{24}$$

$$\xi^I = \left[\underline{\xi}, \overline{\xi}\right] = \xi_0 + \Delta\xi\widehat{e}_7^I = \xi_0\left(1 + \Delta\chi_\xi \widehat{e}_7^I\right). \tag{25}$$

The interval loading and structural parameters can be collected into the following vector:

$$\mathbf{x}^I = \left\{\left(\mathbf{x}_S^I\right)^{\mathrm{T}}\left(\mathbf{x}_L^I\right)^{\mathrm{T}}\right\}^{\mathrm{T}}. \tag{26}$$

By interval extension, the maximum response in Eq. (8) is rewritten as follows:

$$q_{\max}^I = G_q^I q_{\mathrm{m}}^I \tag{27}$$

where, according to Eq. (15):

$$q_{\max}^I \equiv q_{\max}\left(\mathbf{x}^I\right) \equiv q_{\max}\left(\gamma^{*I}, T^I, I_v^I, L_v^I, z_m^I, n_1^I, \xi^I\right) \tag{28}$$

$$G_q^I \equiv G_q\left(\mathbf{x}^I\right) \equiv G_q\left(\gamma^{*I}, T^I, I_v^I, L_v^I, z_m^I, n_1^I, \xi^I\right) \tag{29}$$

$$q_{\mathrm{m}}^I \equiv q_m\left(z_m^I, n_1^I\right). \tag{30}$$

The LB and UB of the interval TGRF and maximum response can be formally expressed as follows:

$$\underline{G}_q = \min_{\mathbf{x}\in\mathbf{x}^I}\{G_q(\mathbf{x})\}; \qquad \overline{G}_q = \max_{\mathbf{x}\in\mathbf{x}^I}\{G_q(\mathbf{x})\} \tag{31}$$

$$\underline{q}_{\max} = \min_{\mathbf{x}\in\mathbf{x}^I}\{q_{\max}(\mathbf{x})\}; \qquad \overline{q}_{\max} = \max_{\mathbf{x}\in\mathbf{x}^I}\{q_{\max}(\mathbf{x})\}. \tag{32}$$

Based on the equations outlined in Section 2.2 (and in Appendix 1), it can be deduced that the functions in Eqs. (28)–(30) exhibit a monotonic dependence on the parameters T^I, I_v^I and ξ^I, and thus achieve their bounds for suitable combinations of the endpoints of these parameters. Introducing the sub-vector of interval variables:

$$\widehat{\mathbf{x}}^I = \left\{\gamma^{*I}, L_v^I, z_m^I, n_1^I\right\}^{\mathrm{T}} \tag{33}$$

the LB and UB of the interval TGRF and maximum response can be expressed as follows:

$$\begin{aligned} \underline{G}_q &= \min_{\widehat{\mathbf{x}}\in\widehat{\mathbf{x}}^I}\left\{G_q\left(\underline{T}, \underline{I}_v, \overline{\xi}, \gamma^*, L_v, z_m, n_1\right)\right\}; \\ \overline{G}_q &= \max_{\widehat{\mathbf{x}}\in\widehat{\mathbf{x}}^I}\left\{G_q\left(\overline{T}, \overline{I}_v, \underline{\xi}, \gamma^*, L_v, z_m, n_1\right)\right\} \end{aligned} \tag{34}$$

$$\begin{aligned} \underline{q}_{\max} &= \min_{\widehat{\mathbf{x}}\in\widehat{\mathbf{x}}^I}\left\{q_{\max}\left(\underline{T}, \underline{I}_v, \overline{\xi}, \gamma^*, L_v, z_m, n_1\right)\right\}; \\ \overline{q}_{\max} &= \max_{\widehat{\mathbf{x}}\in\widehat{\mathbf{x}}^I}\left\{q_{\max}\left(\overline{T}, \overline{I}_v, \underline{\xi}, \gamma^*, L_v, z_m, n_1\right)\right\} \end{aligned} \tag{35}$$

where the number of optimization variables is reduced i.e., γ^{*I}, L_v^I, z_m^I and n_1^I. It is worth noticing that the TGRF and maximum response also exhibit a monotonic dependence on the parameter γ^*, except for limited cases of stiff and highly-damped systems, as shown in [25]. Specifically, numerical investigations have shown that for very stiff and damped structures, the equivalent standard deviation C (Eq. (41), Appendix 1) has a decreasing trend up to values of γ^{*I} in a neighbourhood of 0.85, and increases afterwards. Concerning the parameters L_v^I and z_m^I, the way they affect the TGRF and maximum response can be different depending on the height of the structure and its mechanical properties, as will be shown in the next section.

4. Interval bounds of the thunderstorm wind speed model and response sensitivity based on recorded time histories

In this section, the bounds of the parameters of the thunderstorm wind speed model are derived starting from the full-scale measurements of thunderstorm events (Section 4.1). Based on the bounds estimated, the interval EPSD of the nonstationary turbulence is modelled (Section 4.2) as well as the interval maximum dynamic response, for which a sensitivity analysis is performed to assess the influence of the interval parameters (Section 4.3).

4.1. Bounds of the interval wind speed parameters

In order to estimate the uncertain parameters of the EPSD function in Eq. (22), recorded thunderstorm wind speed time histories available at the Department of Civil, Chemical and Environmental Engineering (DICCA) of the University of Genoa are considered. Specifically, a set of 126 time histories recorded by the anemometer network in the High-Tyrrhenian Sea [12,70–72] is analysed, accounting for a temporal window of 10 min. The anemometers are installed in the ports of Genova, La Spezia, Savona and Livorno and are located at different heights, no lower than 10 m above the ground. More details on the characteristics of the anemometer network can be found in [24]. From this set of data, the relevant parameters – i.e. $\gamma*$, T, L_v, I_v– are extracted and analysed. Each record of the wind speed is decomposed as shown in Eqs. (1) and (2). The reduced turbulent fluctuation $\widetilde{v}'$, treated as a stationary Gaussian random process, is in turn extracted from the nonstationary turbulent fluctuation v'.

As a first step, the model of slowly-varying mean in Eqs. (2)–(4) is employed to fit the one extracted from the records and to derive the parameters $\gamma*$ and T. Among the 126 time histories, only 109 reasonable values of the parameters $\gamma*$ and T are extracted, while the remaining values were discarded because of the inaccurate fitting of the model.

Successively, from the time-varying turbulence intensity, the average value over 10 min is derived, while the integral length scale is estimated through the approach adopted in [73], which integrates the auto-correlation function and invokes the Taylor hypothesis. For each of the parameters L_v and I_v, 126 values are extracted.

In the context of statistical analysis of experimental data, the initial step is to identify and eliminate outliers, which are defined as those observations that significantly deviate from the other values in the data set. To achieve this, Chauvenet's criterion [60,61] was applied to the

data extracted from the thunderstorm time histories. According to Chauvenet's criterion, the data that did not comply with the assumed criterion were discarded. As a result of the application of the Chauvenet's criterion, 3 values of the parameters T and I_v were discarded. The flow chart in Fig. 3 summarizes the steps of this procedure.

Starting from the available experimental data, different approaches have been proposed in the literature to select the range of variability of the uncertain parameters [74–76]. Considering the worst-case scenario, that is, assuming the full range of measured values would result in excessive variability in the uncertain wind speed parameters and overly conservative estimates of the response, even after removing the outliers. To obtain tighter ranges of variability, in this paper, the LB and UB of the thunderstorm parameters are defined considering the respective percentiles of 10% and 90% of the measured data.

Fig. 4 shows the values of the parameters $\gamma*$, T, L_v, and I_v extracted from the thunderstorm dataset together with their respective ranges (light grey) between the lower and upper bounds.

It is worth emphasizing that, even after removing the outliers and considering the 10% and 90% percentiles of the data, the ranges of variability of the parameters remain very wide (Table 1).

Concerning the height of the tip of the nose-shape profile z_m [77,78], this parameter is quite uncertain due to the lack of data regarding the thunderstorm mean wind speed vertical profile. Studies carried out from LiDAR measurements confirmed the significant variation of this parameter, pointing out that the nose shape of the profile lasts only during the intense phase of the outflow [79]. In previous studies, focused on the dynamic response of structures to thunderstorm winds, a range of values $z_m \in [25,100]$m is assumed [80]. Since no information is available from the considered anemometric data, the range specified in [80] is assumed in the present study.

Table 1 reports the quantities associated with the uncertain loading parameters extracted from the thunderstorm dataset and treated with Chauvenet's criterion: LB $\underline{x}_k$; UB $\overline{x}_k$; midpoint or nominal value $x_{k,0}$ (Eq. (12)); deviation amplitude Δx_k (Eq. (13)), and normalized deviation amplitude $\Delta\chi_k$ (Eq. (14)) [34].

Table 1 demonstrates a significant variation in the selected parameters, indicating a substantial change in the associated EPSD function of the thunderstorm wind speed. Clearly, the main parameters in Table 1 which characterize the EPSD of the thunderstorm wind speed, should be suitably modelled as nondeterministic quantities. In Fig. 5, some realizations of the interval modulating function $\gamma^I(t)$ (Eq. (3)) are plotted, setting the interval parameters γ^{*I} (Fig. 5a) and T^I (Fig. 5b) equal to their LB, UB and midpoint.

Fig. 5 shows how the uncertainties in the parameters γ^{*I} and T^I affect

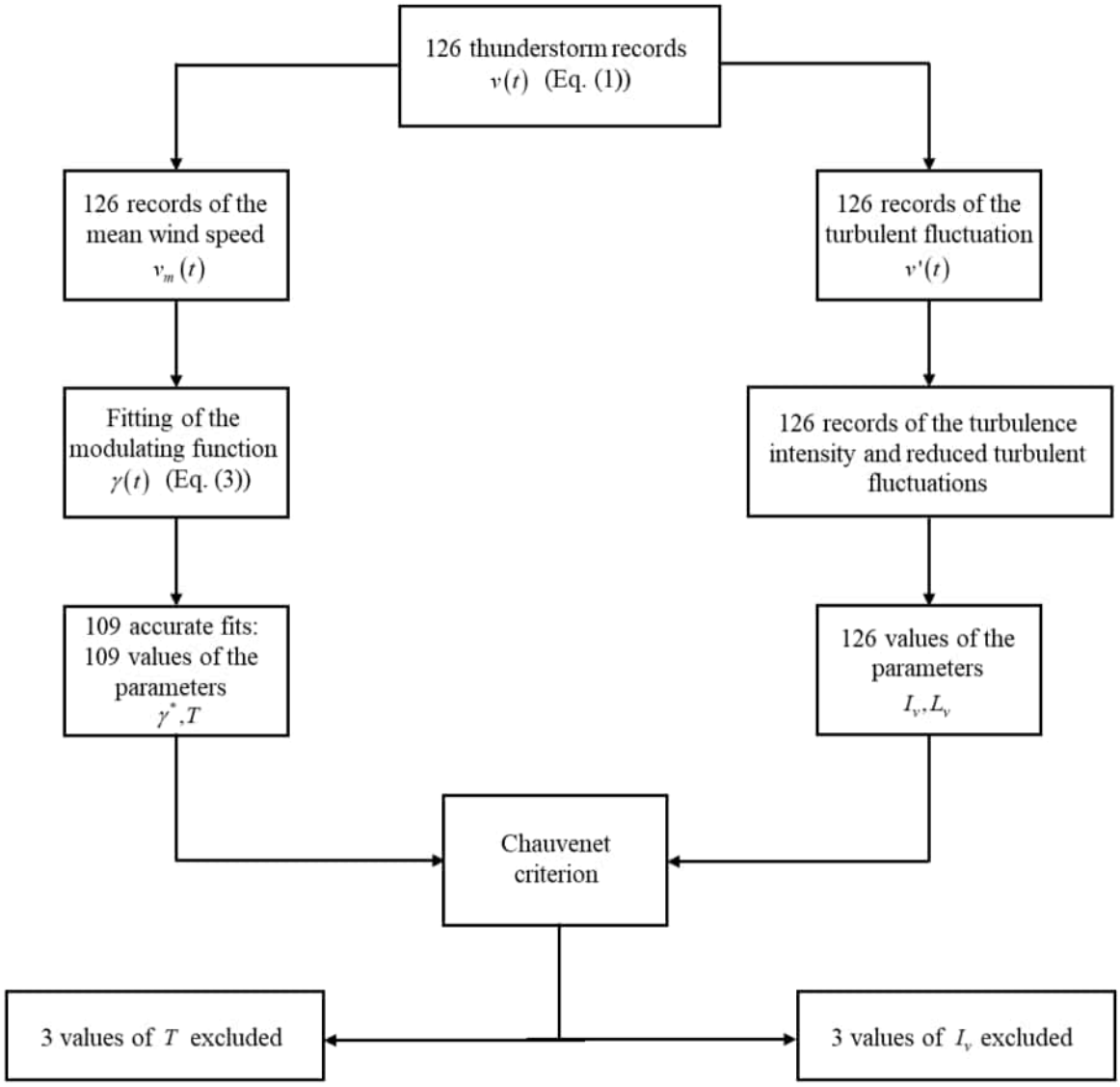

Fig. 3. Flow chart summarizing the analysis of recorded thunderstorm wind speed time histories.

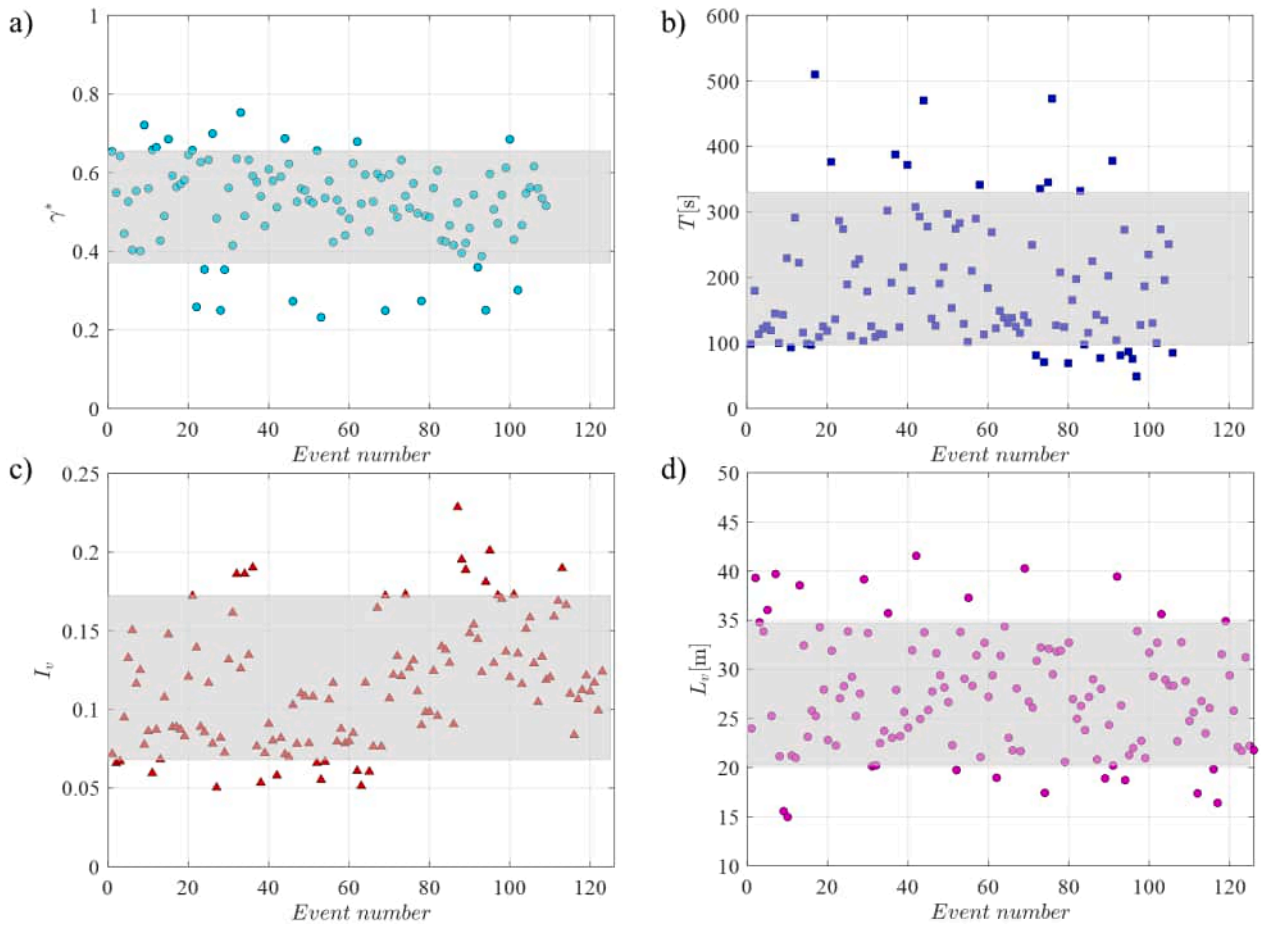

Fig. 4. Values of the parameters (a) γ^*, (b) T, (c) I_v, and (d) L_v, and their respective ranges (light grey) between the lower and upper bounds.

Table 1
Lower and upper bounds, midpoint, deviation amplitude, and normalized deviation amplitude of the interval variables associated with the wind speed.

Parameter	$\underline{x}_k$	$\overline{x}_k$	$x_{k,0}$	Δx_k	$\Delta\chi_k$
$\gamma*$	0.371	0.655	0.513	0.142	0.277
T[s]	97.073	329.464	213.269	116.196	0.549
I_v	0.068	0.172	0.120	0.052	0.433
L_v[m]	20.261	34.732	27.496	7.236	0.263
z_m[m]	25	100	62.5	37.5	0.60

the modulating function $\gamma(t)$, by increasing its constant parts and width, respectively. Fig. 6 plots the realizations of the interval vertical profiles $\alpha^I(z)$ (Eq. (4)) and $\theta^I(z)$ (Eq. (6)) obtained by fixing the interval parameter z_m^I equal to its LB, UB, and midpoint.

Clearly, the uncertainty associated with z_m^I affects the profiles mainly at higher heights, while its effect at lower elevations is less evident.

Fig. 7 plots the interval PSD of the reduced fluctuations $S_{\tilde{v}}^I(z,n)$ (Eq. (7)) evaluated at $z=\overline{z}_m$ (where the larger discrepancies among the profiles are observed in Fig. 6) and fixing the interval parameters z_m^I and L_v^I at their LB, UB, and midpoint.

Fig. 7 shows how changes in parameters z_m^I and L_v^I lead to a shift in the PSD harmonic content. In particular, moving from the lower to the upper bound of the parameters z_m^I (Fig. 7a) and L_v^I (Fig. 7b), the PSD harmonic content moves towards higher frequencies and lower frequencies, respectively.

4.2. Bounds of the interval EPSD model

Based on the bounds of the interval parameters outlined in Section 4.1, the bounds of the interval EPSD model in Eq. (22) can be derived. As an example, Fig. 8 plots the interval EPSD of the nonstationary turbulence v', $S_{v'}^I(z,t,n)$, (Eq. (22)), for the lower and upper bounds of the parameters γ^{*I}, T^I, z_m^I, I_v^I and L_v^I (see Eq. (21)), and their midpoint.

Fig. 8 shows that on moving from the lower to the upper bounds of the parameters γ^{*I}, T^I, and I_v^I, the interval EPSD significantly increases. According to the analytical models outlined in Section 2.1, it is evident that the EPSD is a monotonic increasing function of γ^{*I}, T^I and I_v^I. Thus, the bounds of the EPSD can be expressed as follows:

$$\underline{S}_{v'}(z,t,n) = \min_{L_v\in L_v^I, z_m\in z_m^I}\left\{S_{v'}\left(z,t,n;\underline{\gamma}^*,\underline{T},\underline{I}_v,L_v,z_m\right)\right\} \tag{36}$$

$$\overline{S}_{v'}(z,t,n) = \max_{L_v\in L_v^I, z_m\in z_m^I}\{S_{v'}(z,t,n;\overline{\gamma}^*,\overline{T},\overline{I}_v,L_v,z_m)\}. \tag{37}$$

Nevertheless, the parameters affect the EPSD in different ways and magnitudes. Appendix 2 outlines the effects of each parameter on the EPSD, letting it vary between its lower and upper bounds and fixing the remaining parameters at their midpoint.

4.3. Response sensitivity analysis

In order to investigate the role of the uncertain parameters z_m^I and L_v^I, the TGRF and maximum response, together with their derivatives with respect to these parameters, are plotted for different structural cases with $H>h$ and $H<h$, fixing $\xi=0.2\%$ and varying the natural fre-

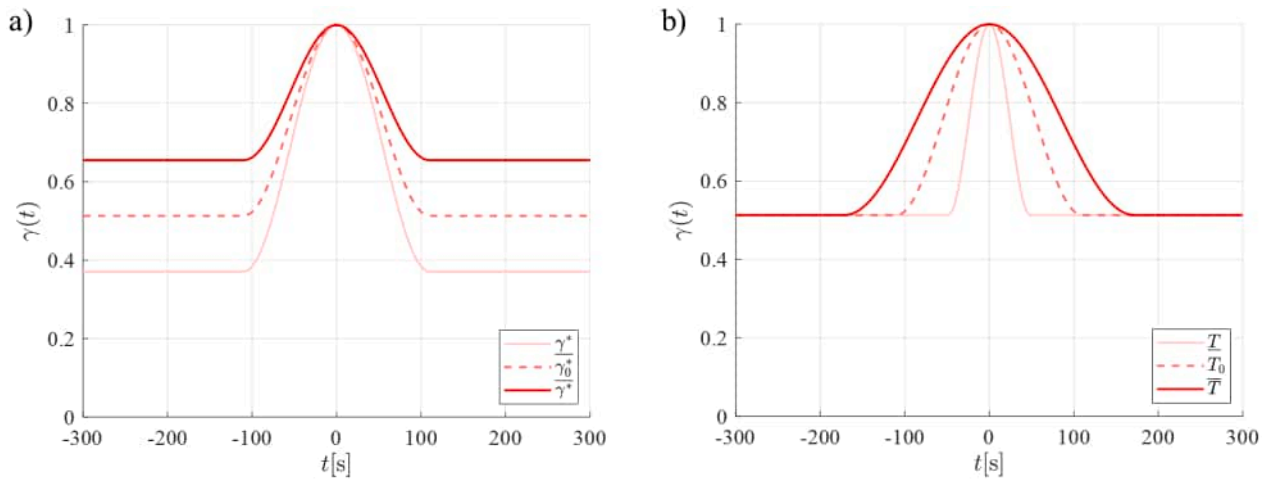

Fig. 5. Interval modulating function of the mean wind speed for different values of the interval variables: (a) $T^I = T_0$, $\gamma^{*I} = \underline{\gamma}^*, \gamma_0^*, \overline{\gamma}^*$; (b) $\gamma^{*I} = \gamma_0^*$, $T^I = \underline{T}, T_0, \overline{T}$.

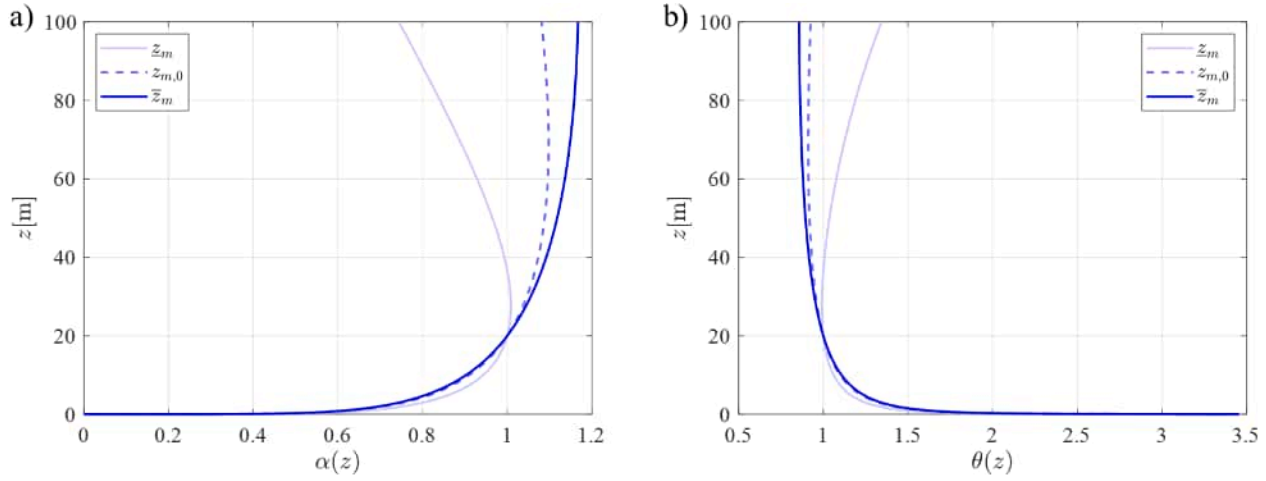

Fig. 6. (a) Interval vertical profile of the mean wind speed $\alpha^I(z)$ and (b) turbulent intensity $\theta^I(z)$ for $z_m^I = \underline{z}_m, z_{m,0}, \overline{z}_m$.

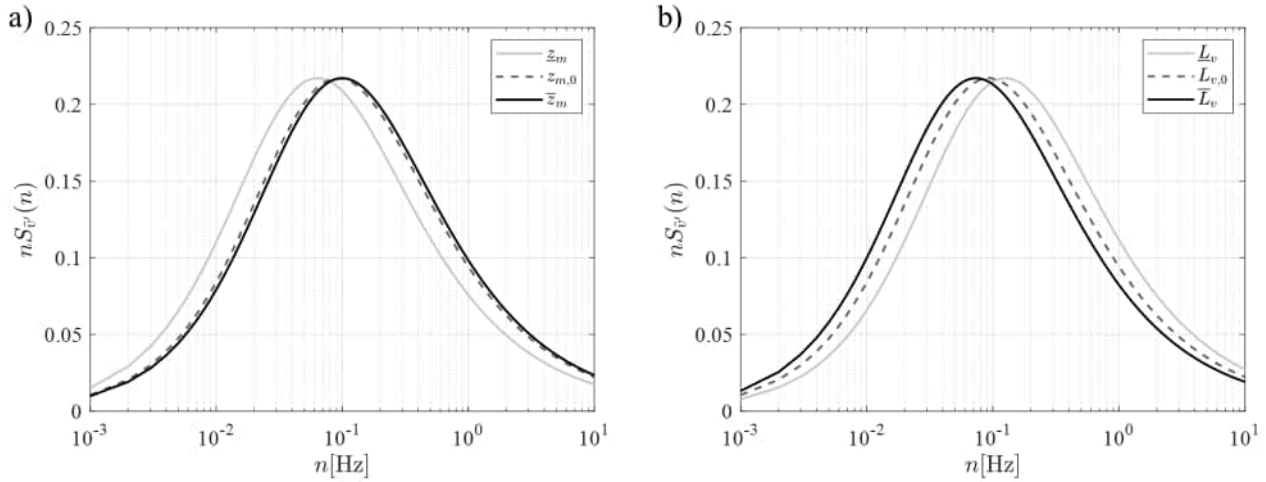

Fig. 7. Interval PSD function of the reduced fluctuations for different values of the interval variables: (a) $L_v^I = L_{v,0}$, $z_m^I = \underline{z}_m, z_{m,0}, \overline{z}_m$; (b) $z_m^I = z_{m,0}$, $L_v^I = \underline{L}_v, L_{v,0}, \overline{L}_v$.

quency $0.05 \leq n_1 \leq 1$. Moreover, in view of the non-monotonic behaviour of the TGRF with the fundamental frequency [21,25], its derivatives with respect to n_1 are also investigated. It is worth pointing out that the analytical formulation of the TGRF and maximum response allows for an analytical expression of their derivatives with respect to all the uncertain parameters involved. However, due to their lengthy and complex formulations, these analytical expressions are omitted, and only their plots are reported.

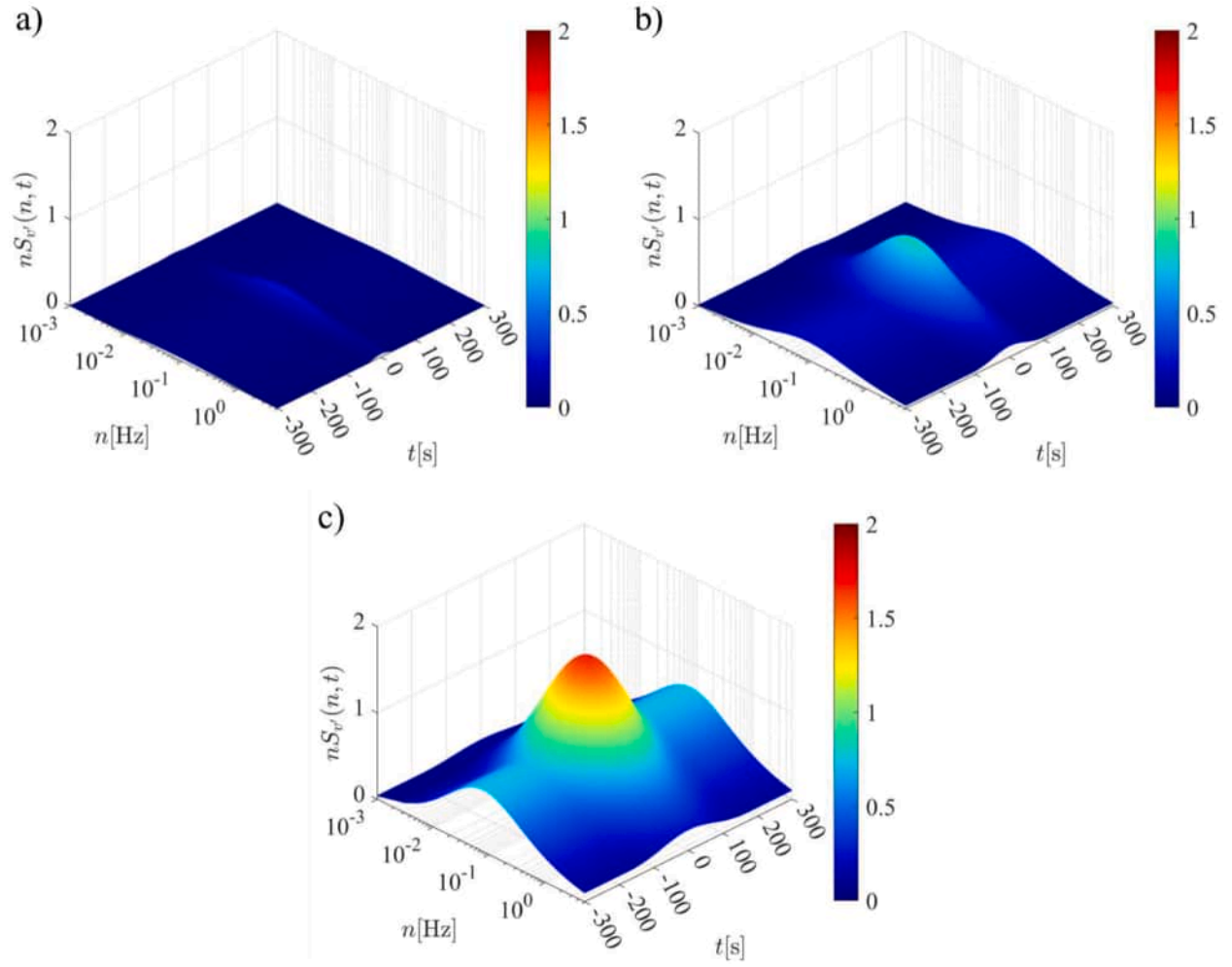

Fig. 8. Interval EPSD of the nonstationary turbulence v' evaluated for different values of the interval variables: (a) $\mathbf{x}_L^I = \underline{\mathbf{x}}_L$; (b) $\mathbf{x}_L^I = \mathbf{x}_{L,0}$; (c) $\mathbf{x}_L^I = \overline{\mathbf{x}}_L$.

Fig. 9 plots the TGRF (Fig. 9a) and the maximum dynamic response (Fig. 9b) for a structure with $H < h$ as functions of $z_m \in z_m^I$ and $n_1 \in [0.05,\ 1]$ Hz. In addition, to better analyse the sensitivity of these quantities with respect to the two parameters, their derivatives with respect to z_m and n_1 are plotted in Fig. 9c–f. Fig. 9a shows the non-monotonic behaviour of the TGRF with n_1 and the small influence of z_m on the TGRF, which is observed to slightly increase on increasing z_m, being the derivative small but positive (Fig. 9c). Indeed, the TGRF is very sensitive to n_1, with the respective derivative that changes the sign from positive to negative (Fig. 9e). Focusing on the maximum response, no change of sign in the derivatives is observed (Fig. 9d, f), assessing a monotonic behaviour with both the parameters. However, it is worth noticing that, differently from the TGRF case, the derivative with respect to z_m is negative. Moreover, the magnitude of the derivatives reduces on increasing z_m and n_1, tending to zero. This result suggests that the impact of the uncertainties of these two parameters on the TGRF and maximum response reduces for higher values of z_m when dealing with a low-rise and stiff structure.

Similar plots are shown in Fig. 10 considering a structure with $H > h$. Differently from the previous case, the non-monotonic behaviour of the TGRF with n_1 is now confined to very low frequencies (Fig. 10a and e). The major difference from the previous case lies in the sign of the derivatives with respect to z_m. Indeed, now the TGRF reduces on increasing z_m and the maximum response increases (Fig. 10c and d), especially for flexible systems. It is worth pointing out that, as observed in Fig. 9, the magnitude of the derivatives with respect to z_m remains small, especially for the maximum response.

Fig. 11 plots the TGRF (Fig. 11a) and the maximum dynamic response (Fig. 11b) as functions of $L_v \in L_v^I$ and $n_1 \in [0.05,\ 1]$ Hz for a structure with $H < h$. Furthermore, Fig. 11 plots the derivatives of the TGRF and maximum dynamic response with respect to L_v and n_1.

Besides the non-monotonicity of the TGRF with respect to n_1, Fig. 11a shows that its dependence on the parameter L_v is not particularly significant, although it varies according to the fundamental frequency, as shown in Fig. 11c. In particular, this figure suggests that the TGRF decreases with increasing L_v except for very low values of n_1. Focusing on the maximum response, a dependence on the parameter L_v is observable only at very low values of the fundamental frequency according to the derivative in Fig. 11d, even though the magnitude is very low compared to the case of the TGRF in Fig. 11c. In particular, Fig. 11d suggests that the maximum response decreases with increasing L_v except for very low values of n_1. Concerning the fundamental frequency, the trends observed in Fig. 11 are substantially similar to those in Fig. 9. The results outlined for $H < h$ are also valid for structures with $H > h$, as illustrated in Fig. 12.

Based on these results, it is possible to derive some general considerations. Focusing on the TGRF, it can be argued that it is more affected by the uncertainties related to the interval parameter L_v^I than the ones related to z_m^I. Nevertheless, while a change of sign in the derivatives with respect to L_v is observed moving from a stiff system to a more flexible one, a similar condition associated with z_m can only happen when moving from a low-rise to a high-rise structure. Moreover, while the uncertainties associated with the interval parameter L_v^I affect the maximum response the same way they affect the TGRF, the uncertainties

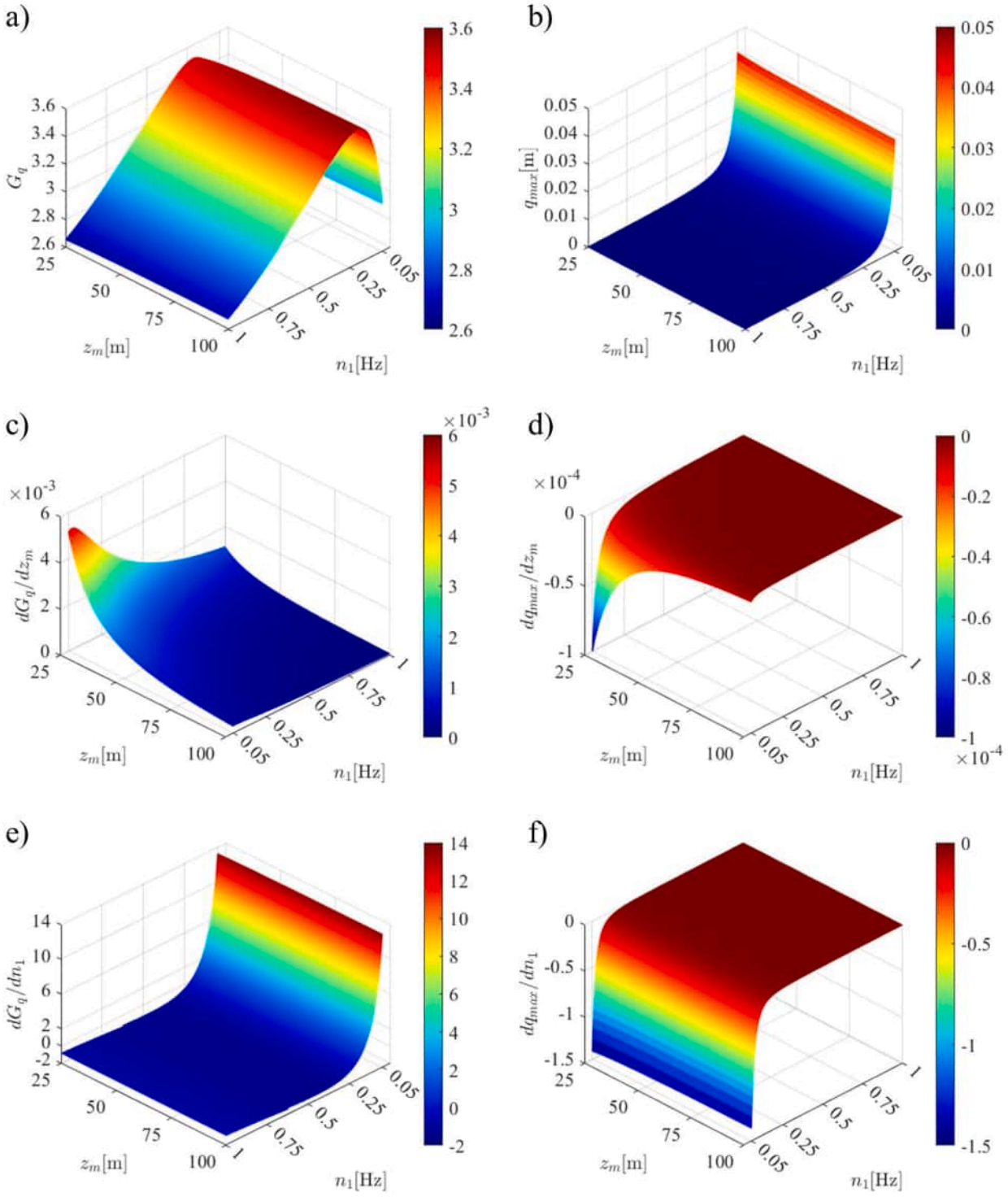

Fig. 9. Structural case study with $H < h$: trends of the (a) TGRF and (b) maximum response and their derivatives with respect to (c),(d) z_m and (e),(f) n_1.

on the interval parameter z_m^I affect differently the TGRF and maximum response due to the role of this quantity in the mean part of the response (Eq. (9)).

5. Numerical application

In this section, interval uncertainty propagation is performed for two real structural systems subjected to the imprecise thunderstorm wind speed presented in Section 3. The main goal is to estimate how uncertainty in the parameters affects the TGRF and the maximum response. First, the structural cases are described, outlining their geometrical and mechanical properties (Section 5.1). Then, the lower and upper bounds of the TGRF and maximum dynamic response are determined, investigating separately the effects of the loading and structural uncertainties (Section 5.2).

5.1. Structures case studies

Two slender vertical structures are considered as case studies: a steel lighting pole (case study 1, Fig. 13a) and a reinforced concrete

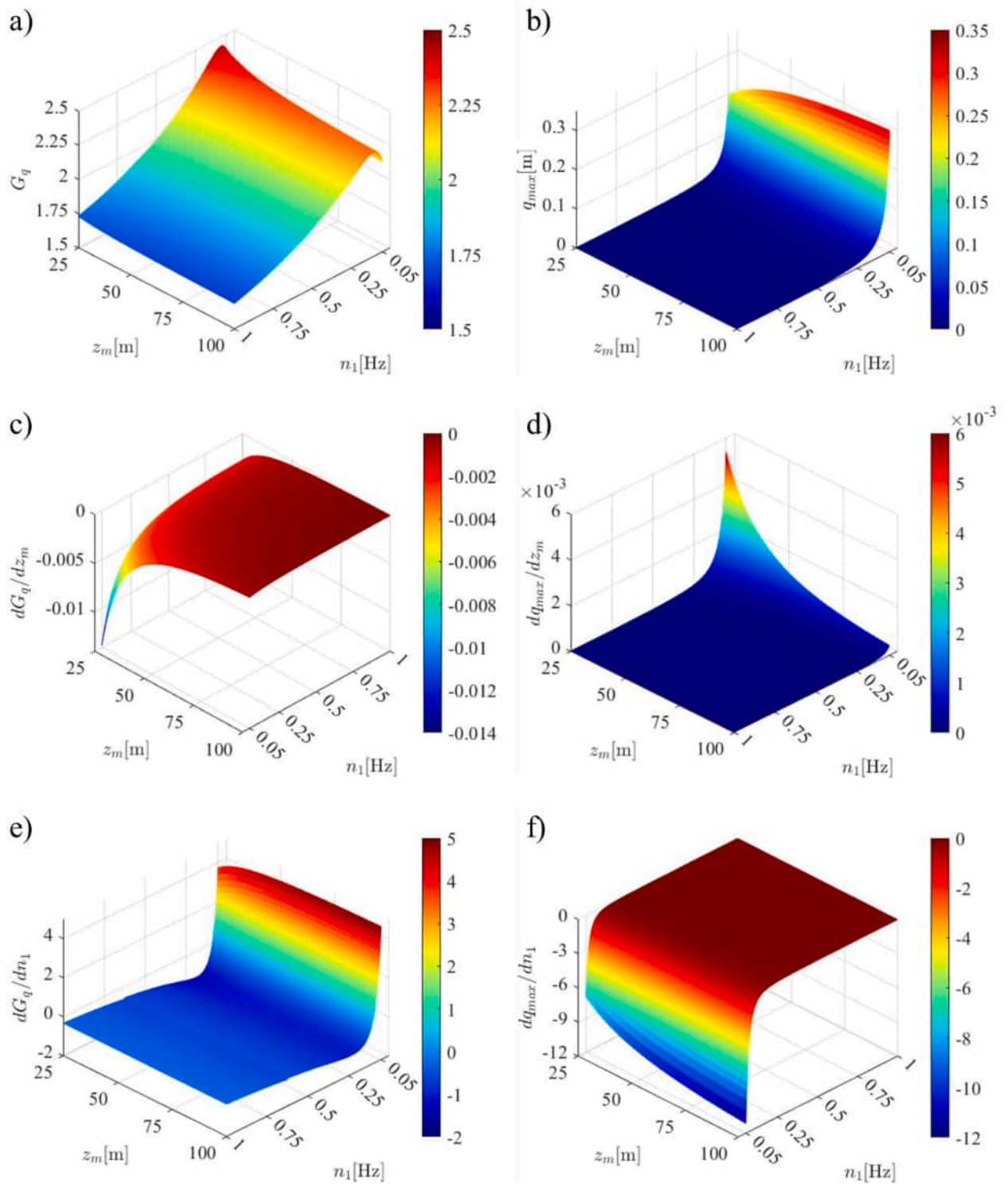

Fig. 10. Structural case study $H > h$: trends of the (a) TGRF and (b) maximum response and their derivatives with respect to (c), (d) z_m and (e),(f) n_1.

telecommunications tower (case study 2, Fig. 13b), both clamped at the base and schematized as cantilever beams. A detailed description of the two structural cases is reported in [18], while in this section, their main geometrical and structural properties are specified. Fig. 13 shows the two structures and their static scheme.

The lighting pole (Fig. 13a) features a shaft with a truncated conical shape and tubular octagonal cross-section, topped with a lighting fixture. The total height above ground is 14 m, and the base and top diameters are 280 mm and 80 mm, respectively. Including the top portion, the structure reaches an overall height of 15.76 m. Given its relatively short height, the pole is classified as a low-rise structure.

The telecommunications tower (Fig. 13b) consists of three stacked shafts for a total height of 98.00 m. The first shaft, extending up to 3.90 m above ground level, is composed of two concentric tubular circular sections connected by six radial walls. The second shaft, ranging from 3.90 to 80.50 m, has a circular tubular cross-section with an outer diameter of 6.50 m and a thickness of 0.50 m. This section features seven steel platforms between 59.50 and 80.50 m supporting transmission

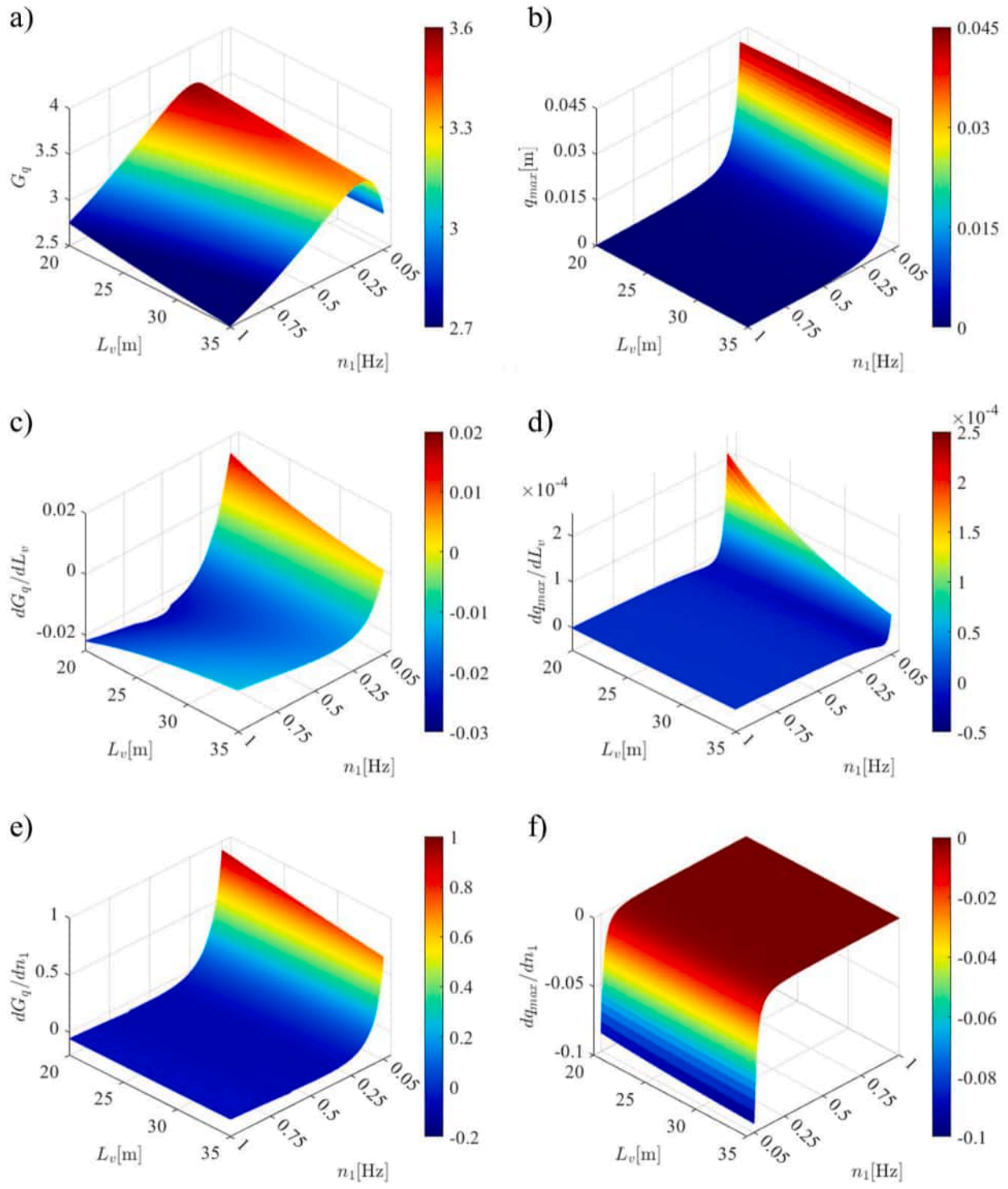

Fig. 11. Structural case study with $H < h$: trends of the (a) TGRF and (b) maximum response and their derivatives with respect to (c),(d) L_v and (e), (f) n_1.

parabolas. The third shaft, from 80.50 to 98.00 m, also has a circular tubular cross-section, with an outer diameter of 3.00 m and a thickness of 0.25 m. In view of its height, the telecommunications tower is categorized as a mid-height structure.

Fig. 14 and Fig. 15 outline the main geometrical and aerodynamic properties of the lighting pole and telecommunications tower, respectively, specifically the mode shape, width and drag coefficient.

It is worth pointing out that the drag coefficient assumed corresponds to a stationary wind field. While appropriate aerodynamic coefficients that account for the transient nature of thunderstorm outflows remain an active area of research, recent studies have indicated that these effects are negligible [81,82].

Table 2 presents the characteristics of both structures, detailing height, the first fundamental frequency, modal mass, and damping ratio [18].

It is worth noticing that the values of the damping ratio, as reported in [18], are assumed according to the material of the structure, respectively, steel for the lighting pole and reinforced concrete for the telecommunications tower. In order to investigate the propagation of uncertainties related to the structural parameters on the TGRF and

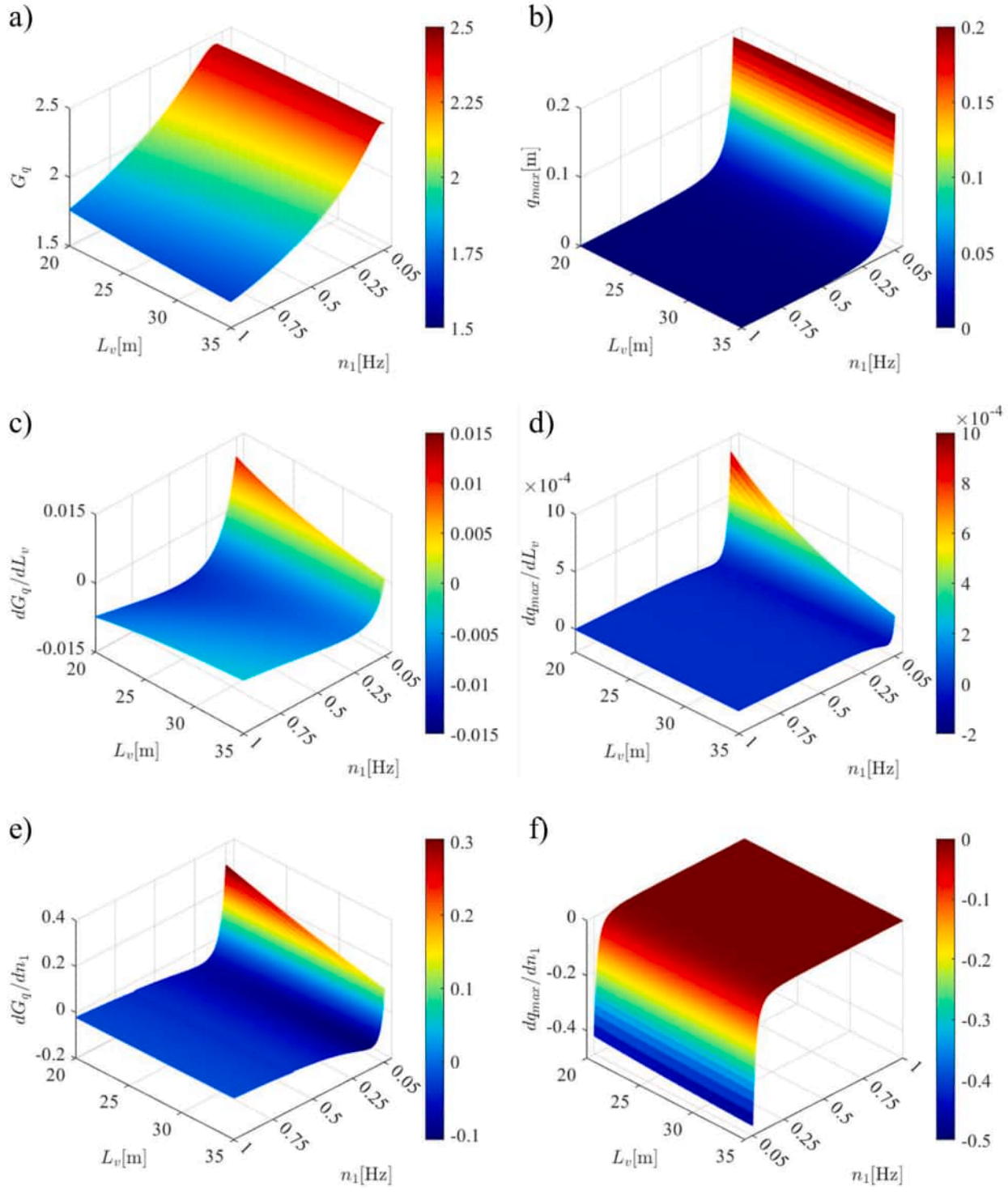

Fig. 12. Structural case study with $H > h$: trends of the (a) TGRF and (b) maximum response and their derivatives with respect to (c),(d)L_v and (e),(f)n_1.

maximum response, a certain level of uncertainty is assumed for the first modal frequency and damping ratio of the two structures. For the latter in particular, an uncertainty of 30% on the actual value is estimated starting from previous studies carried out by [68,69]. Instead, for the fundamental frequency, an error of 5% is assumed a priori, based on the discrepancies outlined in a previous study between values of fundamental frequencies obtained from numerical and experimental analyses [67]. By treating these two parameters as interval variables, their lower and upper bounds as well as their midpoints, deviation amplitude, and normalized deviation amplitude are summarized in Table 3.

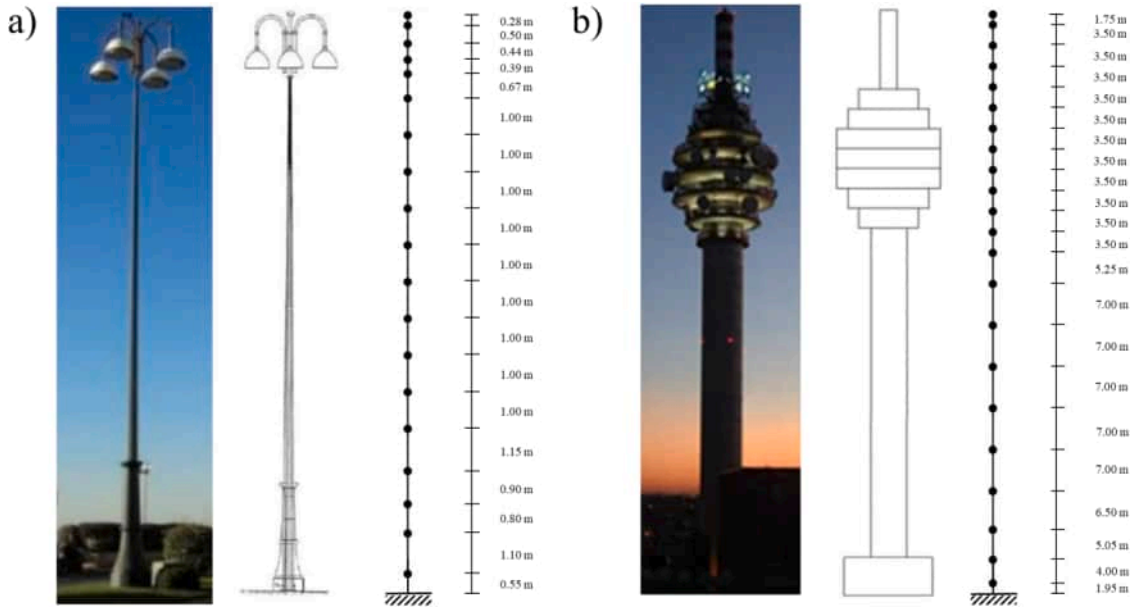

Fig. 13. Structural case study and discretization: Lighting pole (a); Telecommunications tower (b).

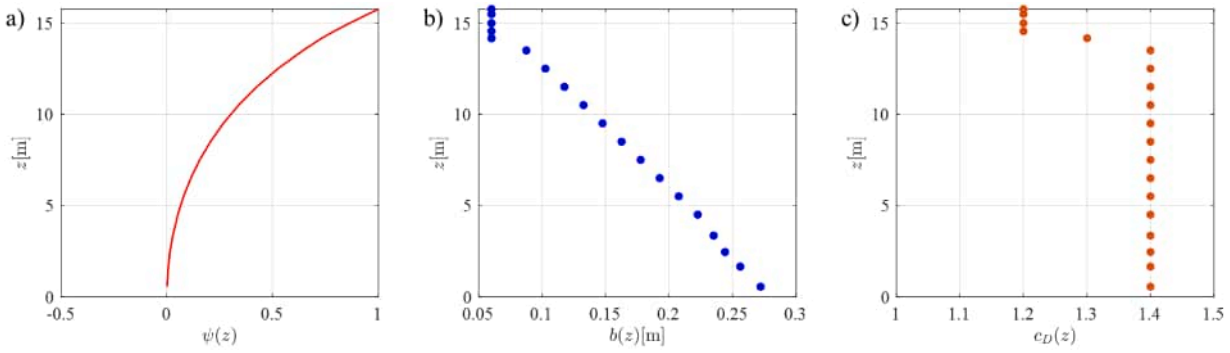

Fig. 14. Properties of the lighting pole: (a) mode shape, (b) width, and (c) drag coefficient.

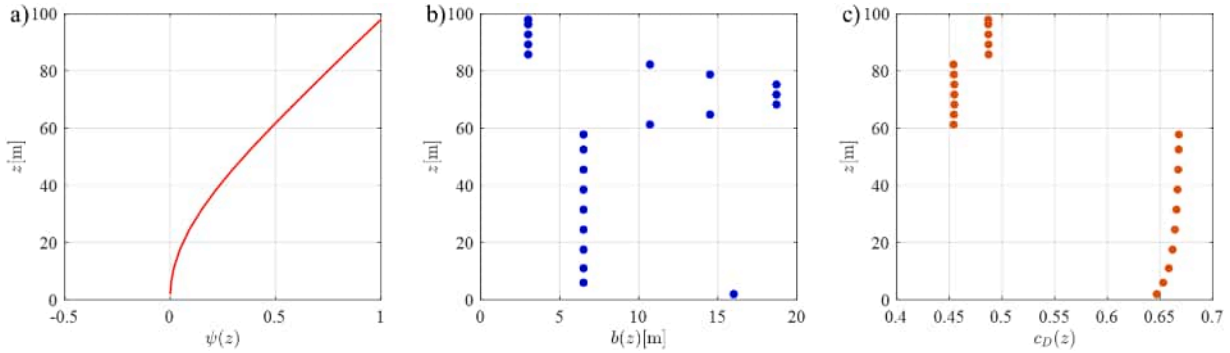

Fig. 15. Properties of the telecommunications tower: mode shape (a), width (b) and drag coefficient (c).

Table 2
Structural properties of the case studies considered.

Structural case study	H [m]	n_1 [Hz]	m_1 [kg]	ξ
Case 1: Lighting pole	15.76	0.528	164.37	0.002
Case 2: Telecommunications tower	98	0.494	482989.76	0.005

5.2. Intervals of TGRF and maximum dynamic response

In this section, the lower and upper bounds of the TGRF and maximum dynamic response are estimated based on the intervals of the uncertain parameters outlined in Tables 1 and 3. The bounds are first estimated focusing on one interval parameter at a time while fixing the others at their midpoints, to investigate the effect of each uncertain parameter. Successively, only the wind loading parameters are modelled as interval variables, keeping the structural ones fixed at their nominal

Table 3
Lower and upper bounds, midpoint, deviation amplitude, and normalized deviation amplitude of the interval variables associated with structural case studies.

Case study	Parameter	$\underline{x}_k$	$\overline{x}_k$	$x_{k,0}$	Δx_k	$\Delta\chi_k$
1	n_1 [Hz]	0.502	0.554	0.528	0.026	0.05
	ξ	0.0016	0.0024	0.002	0.0004	0.30
2	n_1 [Hz]	0.469	0.519	0.494	0.025	0.05
	ξ	0.004	0.006	0.005	0.001	0.30

values. This case is named Loading Uncertainties (LU). Then, only the structural parameters are let to vary in their range with the wind loading parameters fixed at their midpoint. This case is referred to as Structural Uncertainties (SU). Finally, all the parameters are considered uncertain, referring to this case as Full Uncertainty (FU). By operating in this way, the influence of the parameters in determining the uncertainties on the TGRF and maximum response is explored. Moreover, the lower and upper bounds are determined by considering an increasing degree of uncertainty on the involved parameters, according to the following definition of interval variable (Eq. (11))

$$x_k^I = x_{k,0}\left(1+\mu\Delta\chi_k\widehat{e}_k^I\right) \tag{38}$$

where the coefficient $\mu \in [0,1]$ measures the degree of uncertainty.

Specifically, for each value of the coefficient μ, the lower and upper bounds of the TGRF and maximum response in Eqs. (29) and (28) are estimated numerically through an optimization procedure with respect to the uncertain parameters, constrained to belong to their prescribed intervals (see Eqs. (31) and (32)).

It is worth noticing that the realizations of the interval variables T^I, I_v^I and ξ^I which yield the bounds of the TGRF and maximum response are indicated in Eqs. (34) and (35). Instead, the role of the parameters γ^{*I}, L_v^I, z_m^I and n_1^I is case-dependent according to the structural properties, as shown in Section 4. Specifically, concerning the parameter γ^{*I}, based on the results outlined in [25], usually the LB (UB) of the TGRF and maximum response are achieved in conjunction with the LB (UB) of this parameter. Focusing on the parameters L_v^I and n_1^I, based on the trends outlined in Section 4 for the selected case studies, it can be stated that the LB (UB) of the TGRF and maximum response are obtained for the UB (LB) of these quantities. Finally, concerning the parameter z_m^I and taking into account that case study 1 can be considered a low-rise structure and case study 2 a high-rise structure, it can be stated that the LB (UB) of the TGRF are obtained for the LB (UB) of z_m^I for case study 1 and its UB (LB) for case study 2; instead the LB (UB) of the maximum response corresponds to the UB (LB) of z_m^I for case study 1 and to its LB(UB) for case study 2. Based on these observations, for the selected case studies, Eqs. (34) and (35) provide the following analytical expressions of the bounds of the TGRF and maximum dynamic response under FU:

$$\begin{aligned}
\underline{G}_{q,1} &= G_{q,1}\left(\underline{\gamma}^*,\underline{T},\underline{I}_v,\overline{L}_v,\underline{z}_m,\overline{\xi},\overline{n}_1\right);\\
\overline{G}_{q,1} &= G_{q,1}\left(\overline{\gamma}^*,\overline{T},\overline{I}_v,\underline{L}_v,\overline{z}_m,\underline{\xi},\underline{n}_1\right);\\
\underline{q}_{\max,1} &= q_{\max,1}\left(\underline{\gamma}^*,\underline{T},\underline{I}_v,\overline{L}_v,\overline{z}_m,\overline{\xi},\overline{n}_1\right);\\
\overline{q}_{\max,1} &= q_{\max,1}\left(\overline{\gamma}^*,\overline{T},\overline{I}_v,\underline{L}_v,\underline{z}_m,\underline{\xi},\underline{n}_1\right)
\end{aligned} \tag{39}$$

$$\begin{aligned}
\underline{G}_{q,2} &= G_{q,2}\left(\underline{\gamma}^*,\underline{T},\underline{I}_v,\overline{L}_v,\overline{z}_m,\overline{\xi},\overline{n}_1\right);\\
\overline{G}_{q,2} &= G_{q,2}\left(\overline{\gamma}^*,\overline{T},\overline{I}_v,\underline{L}_v,\underline{z}_m,\underline{\xi},\underline{n}_1\right);\\
\underline{q}_{\max,2} &= q_{\max,2}\left(\underline{\gamma}^*,\underline{T},\underline{I}_v,\overline{L}_v,\underline{z}_m,\overline{\xi},\overline{n}_1\right);\\
\overline{q}_{\max,2} &= q_{\max,2}\left(\overline{\gamma}^*,\overline{T},\overline{I}_v,\underline{L}_v,\overline{z}_m,\underline{\xi},\underline{n}_1\right)
\end{aligned} \tag{40}$$

where the subscripts 1 and 2 relate to the case study considered. It is worth emphasizing that the bounds are achieved for suitable combinations of the endpoints of the interval parameters, due to the monotonic behaviour of the TGRF and maximum dynamic response in both case studies. Furthermore, the analytical estimates of the bounds in Eqs. (39) and (40) are in perfect agreement with the results of the numerical optimization.

Figs. 16 and 17 plot the trends of the LB and UB of the TGRF (Figs. 16a and 17a) and maximum dynamic response (Figs. 16b and 17b) for each case study, considering only one interval parameter at a time and fixing the others at their respective nominal values, on varying the degree of uncertainty.

It can be deduced that, for both the case studies considered, the major contribution to the LB and UB of the TGRF is given by the turbulence intensity I_v^I. A non-negligible impact is also observed for the parameter T^I, which implies an uncertainty comparable to the one of the damping ratio for the UB, while a greater contribution is observed for the LB. Focusing on case 1 (Fig. 16a), it is observed that the LB and UB of the TGRF are similarly affected by the parameters γ^{*I}, L_v^I and ξ^I, while the smallest contribution to the uncertainty is given by the parameters z_m^I and n_1^I. Concerning case 2 (Fig. 16b), the parameter L_v^I appears to be less impactful on the TGRF compared to case 1, consistent with the result shown in Fig. 12. As a general consideration, it is worth noticing the impact that some uncertain parameters have on the global output uncertainty relative to their normalized deviation amplitude (Table 1).

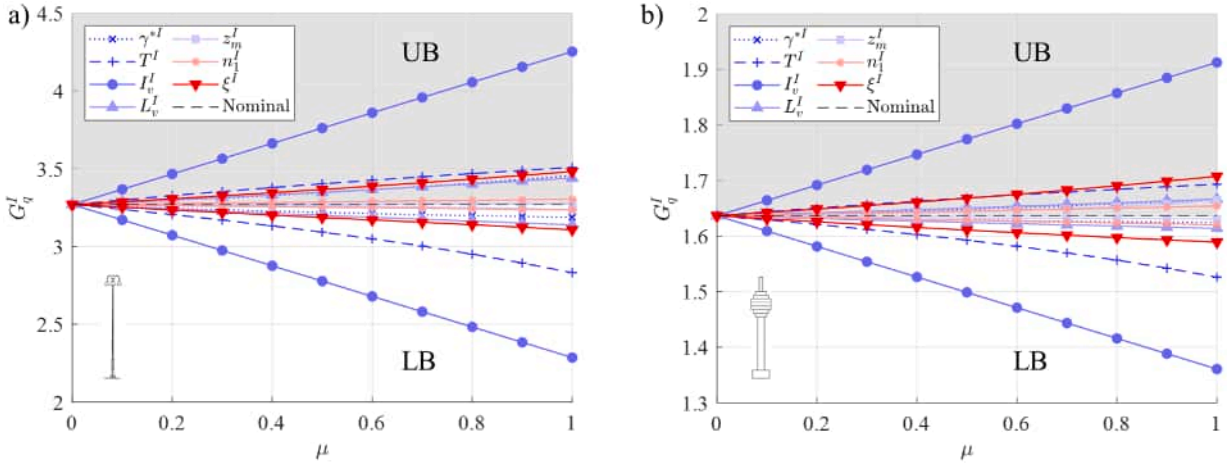

Fig. 16. LB and UB of the TGRF estimated considering one interval parameter at a time: (a) case study 1; (b) case study 2.

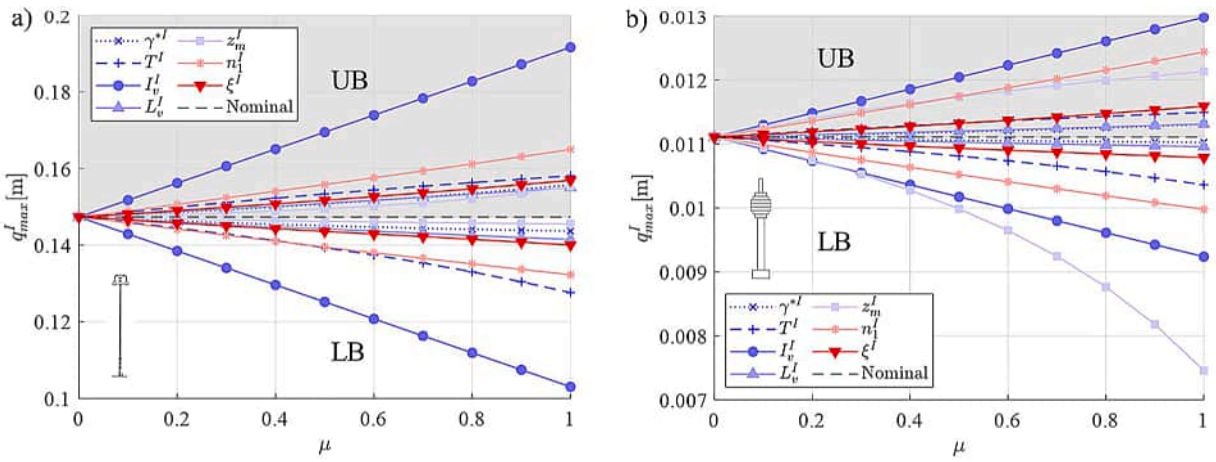

Fig. 17. LB and UB of the maximum response estimated considering one interval parameter at a time: (a) case study 1; (b) case study 2.

Indeed, despite the parameters T^I and z^I_m are those with the greatest normalized deviation amplitude, their impact on the uncertainty of the TGRF is lower than that of other parameters, such as I^I_v. This is particularly significant in case 2 (Fig. 16b) where the influence of z^I_m is very small if compared with its normalized deviation amplitude in Table 1.

Fig. 17 shows that the role of the turbulence intensity I^I_v is still predominant also in determining the LB and UB of the maximum response, with the exception of case 2 where the LB is significantly affected by the parameter z^I_m. In particular, the role of this latter parameter changes considerably from case 1 to 2, becoming more influential for the taller structure (Fig. 17b) in accordance with the magnitude of its derivatives plotted in Figs. 9d and 10d. It can also be observed that the fundamental frequency n^I_1 affects the maximum response more than the damping ratio, with trends of the LB close to those given by T^I in case 1 (Fig. 17a) and trends of the UB similar to those found for the parameter z^I_m in case 2 (Fig. 17b). Finally, the interval parameters γ^{*I}, L^I_v and ξ^I show a similar influence on the LB and UB, with a more significant role for case 1 compared to case 2. Similarly to Fig. 16, the impact of the parameters T^I and z^I_m, characterized by a large normalized deviation amplitude, is actually low for the maximum response. The only difference is observed for case 2 (Fig. 17b) where z^I_m has a larger impact on the uncertainties of the maximum response with respect to the TGRF in Fig. 16b but still smaller than the uncertainties provided by I^I_v. Instead, it can be observed that despite the larger normalized deviation amplitude of the damping ratio with respect to the fundamental frequency (Table 1), the uncertainty of the maximum response is largely affected by this latter.

Figs. 18 and 19 plot the trends of the LB and UB of the TGRF and maximum response obtained considering only the LU, the SU and finally all the uncertain parameters together (FU).

It can be observed that both the TGRF and maximum dynamic response are more affected by the uncertainties associated with the wind loading parameters in both the structural cases considered. This is evident for the TGRF (Fig. 18), and it is mainly due to the uncertainties on the turbulence intensity, as shown in Fig. 16. Focusing on the maximum response (Fig. 19), it can be noticed that the impact of the uncertainties associated with the wind loading is still crucial compared to those of the structural parameters. However, the uncertainties related to the structural parameters have a more significant impact than those observed for the TGRF. This result can be related to the more impactful role of the fundamental frequency as shown in Fig. 17. Finally, the trends of the LB and UB associated with the FU suggest that the combined effects of the LU and SU can lead to a maximum response up to twice the nominal value (Fig. 19a), and the main contribution is given by the LU. Thus, neglecting uncertainties may lead to a significant underestimation of the maximum response compared to the worst-case scenario (UB). This result highlights the importance of accurately estimating the wind loading parameters in engineering practice, especially those which majorly affect the LB and UB of the TGRF and maximum response.

For comparison purposes, the influence of uncertainties on the TGRF and maximum response is also investigated by modelling the uncertain structural and loading parameters x_k ($k = 1, \ldots, 7$) as independent

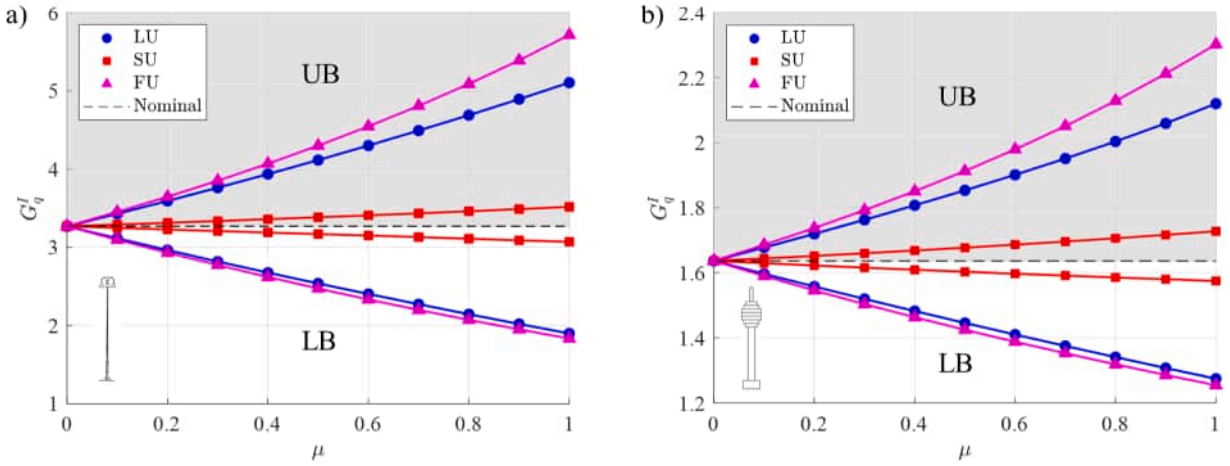

Fig. 18. Bounds of the TGRF for the (a) lighting pole and (b) telecommunications tower.

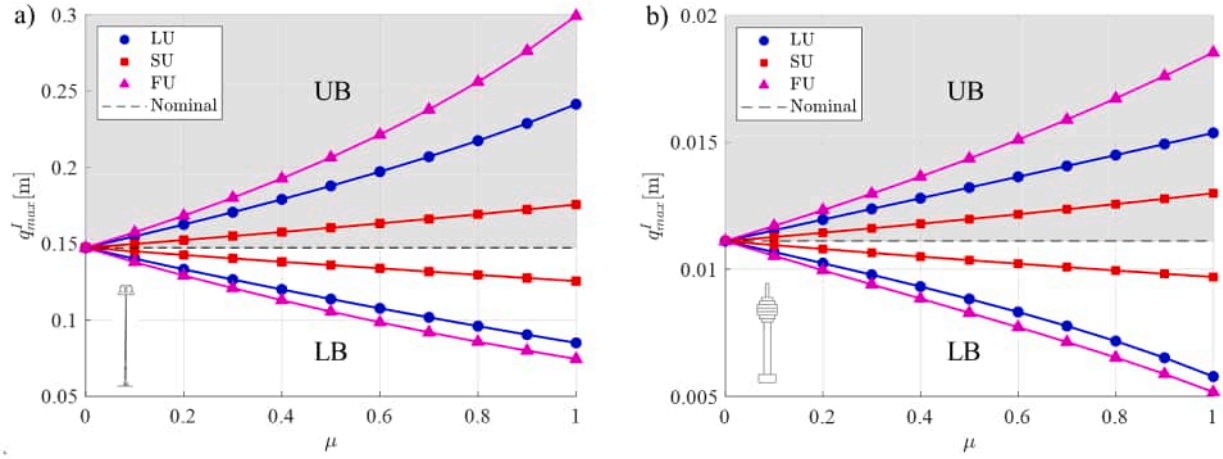

Fig. 19. Bounds of the maximum dynamic response for the (a) lighting pole and (b) telecommunications tower.

random variables characterized by a uniform distribution over the pertinent intervals $[\underline{x}_k, \overline{x}_k]$ (see Tables 1 and 3). The mean values, μ_{G_q} and $\mu_{q_{\max}}$, and standard deviations, σ_{G_q} and $\sigma_{q_{\max}}$, of the TGRF and maximum response are estimated by applying Monte Carlo Simulations employing $N = 10^6$ samples of the random parameters. Figs. 20 and 21 show the comparison between the LB and UB of the interval TGRF and maximum response obtained assuming FU and the statistical confidence intervals $\mu_{G_q} \pm 3\sigma_{G_q}$ and $\mu_{q_{\max}} \pm 3\sigma_{q_{\max}}$ provided by probabilistic analysis.

For both case studies, it can be observed that the interval approach generally provides more conservative estimates compared to the statistical confidence interval associated with uniformly distributed uncertain parameters, especially concerning the worst-case scenario (UB). Obviously, the difference between the results obtained using the interval model and the probabilistic approach is affected by the assumed probabilistic distribution, which relies on subjective assumptions when only limited data are available.

6. Conclusions

This study introduced an interval model for thunderstorm wind speed to analyse the propagation of uncertainties characterizing both wind speed and structural parameters on the Thunderstorm Gust Response Factor (TGRF) and maximum dynamic response.

The lower and upper bounds of the wind speed parameters were derived from statistical analyses of a dataset of thunderstorm wind speed records, while the degree of uncertainty of the structural parameters was assumed according to the existing literature.

Relying on the availability of closed-form expressions for the TGRF and maximum dynamic response, an analytical sensitivity analysis was carried out to investigate the relative importance of the uncertain parameters. It was observed that most of the wind and structural parameters are responsible for a monotonic behaviour of the TGRF and maximum response. The results show a significant dependence on the turbulence intensity, the duration of the intense phase of the thunderstorm outflow, and the background wind speed. Moreover, on increasing the duration of the intense phase of the thunderstorm outflow, the background wind speed and the turbulence intensity, the TGRF and maximum response increase.

The sensitivity analysis carried out on two ideal sets of structures showed that the impact of some uncertain parameters, such as the integral length scale and height of the nose profile, changes depending on the fundamental frequency and height of the structure considered. The analyses showed non-monotonic trends for the TGRF on varying the fundamental frequency. Moreover, the magnitude of the derivatives of the TGRF and maximum response allowed us to quantify the sensitivity to the parameters.

To further investigate the effects that each uncertain parameter produces on the TGRF and maximum response, two real structural case studies were considered. Analytical expressions of the bounds of the TGRF and maximum response were derived relying on preliminary investigations on their dependency on the uncertain parameters. The

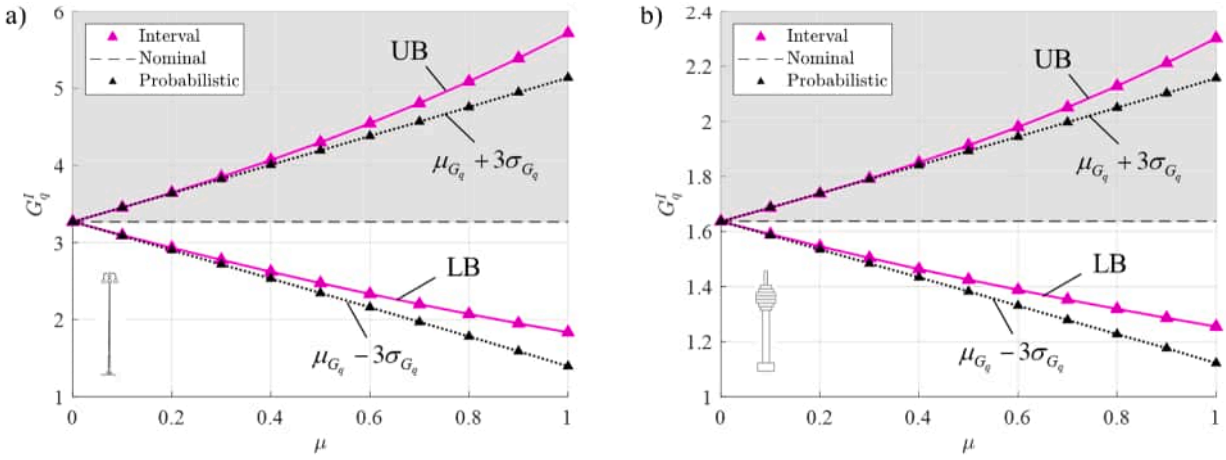

Fig. 20. Comparison between the bounds of the TGRF and the statistical confidence interval provided by probabilistic analysis for the (a) lighting pole and (b) telecommunications tower (FU).

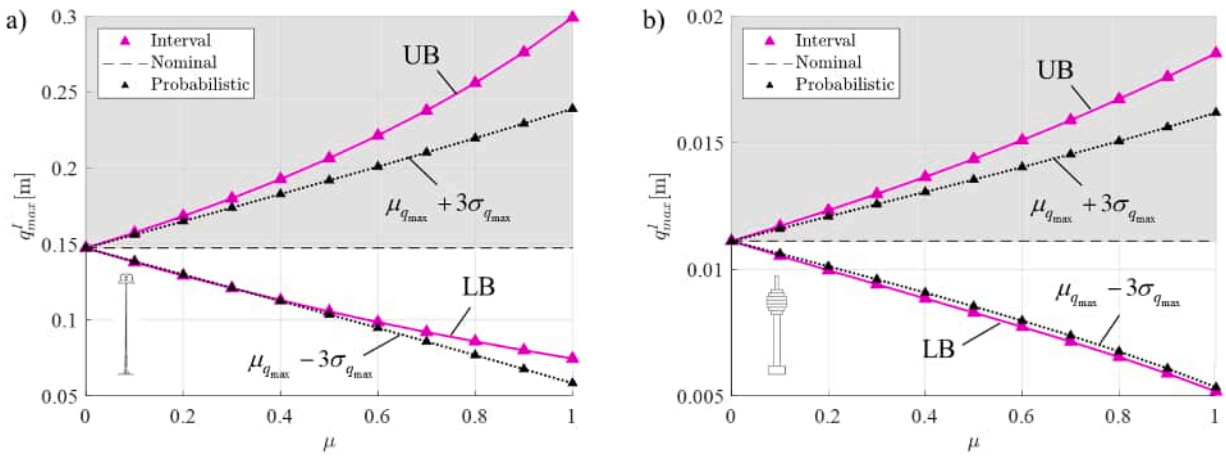

Fig. 21. Comparison between the bounds of the maximum dynamic response and the statistical confidence interval provided by probabilistic analysis for the (a) lighting pole and (b) telecommunications tower (FU).

analyses of the bounds of the TGRF and maximum response allowed us to identify the parameters that mainly affect their uncertainty. It was pointed out that the uncertainties associated with the turbulence intensity have the greatest influence on the uncertainty of both the TGRF and maximum response, even though its normalized deviation amplitude is lower than the one derived for other parameters, such as the duration of the intense phase and height of the nose profile. This latter parameter has a greater impact on the maximum response, as well as the fundamental frequency, while the damping ratio is more significant on the TGRF. Moreover, the uncertainties associated with the height of the nose were observed to have a different influence on low-rise and high-rise structures. In the former case, the bounds of the maximum response are not so sensitive to the uncertainties associated with the height of the nose, while a greater sensitivity is observed for the case of the high-rise structure.

More in general, the uncertainties associated with the wind speed parameters were shown to be crucial in determining the bounds of the TGRF and maximum response, while the role of the mechanical parameters was shown to be less impactful. This result highlights the importance of accurately estimating the wind speed parameters associated with thunderstorm outflows, which are difficult to predict because of the lack of data available for these phenomena.

The proposed extension of the TGRF technique to the interval framework offers a novel and handy method for performing engineering calculations while accounting for imprecision in the thunderstorm wind speed model. Since a limited number of thunderstorm wind speed time histories is typically available, the use of the interval model is advisable for engineering decision-making. In the absence of sufficient data, the classical probabilistic approach should rely on subjective assumptions about the probability density function of the uncertain wind speed parameters, which may lead to unreliable predictions of structural behaviour at the expense of intensive computations. Conversely, the interval model does not provide information about the likelihood of response values between the pertinent bounds and can yield quite conservative results due to its reliance on worst-case uncertain parameter values. Nevertheless, as long as limited information is available, the proposed incorporation of the interval model into the traditional stochastic process description of the thunderstorm wind speed may provide a rational basis for the definition of appropriate safety factors relying on the bounds of the interval maximum response. Should future recordings of thunderstorm events yield a richer dataset, a full probabilistic characterization of the uncertain parameters can be pursued to make suitable engineering decisions. It is also important to highlight a notable gap in the literature regarding the modelling of vertical profiles for wind velocity parameters, such as turbulence intensity and turbulence integral length scale, associated with downbursts. The impact of these profiles on the uncertainty level of structural response is an aspect that deserves further investigation. Moreover, it is important to emphasize that in the present study, the structural uncertainties are accounted for in terms of fundamental frequency and damping ratio. However, uncertainties in the fundamental frequency may stem from variations in the Young's modulus of the material and/or the local geometry of the structure. Therefore, the influence of the structural parameters may be further studied through time-domain analyses on a detailed finite element model involving uncertain material and/or geometrical properties.

CRediT authorship contribution statement

Luca Roncallo: Writing – review & editing, Writing – original draft, Visualization, Validation, Software, Resources, Investigation, Formal analysis, Data curation, Conceptualization. **Alba Sofi:** Writing – review & editing, Methodology, Conceptualization. **Giuseppe Muscolino:** Writing – review & editing, Methodology, Conceptualization. **Federica Tubino:** Writing – review & editing, Supervision, Methodology, Conceptualization.

Declaration of competing interest

The authors declare that they have no known competing financial interests or personal relationships that could have appeared to influence the work reported in this paper.

Acknowledgements

This research is funded by the European Research Council (ERC) under the European Union's Horizon 2020 research and innovation program (grant agreement No. 741273) for the project THUNDERR - Detection, simulation, modelling and loading of thunderstorm outflows

to design wind-safer and cost-efficient structures - supported by an Advanced Grant 2016.

The data used for this research were recorded by the monitoring network set up as part of the European Projects Winds and Ports (grant No. B87E09000000007) and Wind, Ports and Sea (grant No. B82F13000100005), funded by the European Territorial Cooperation Objective, Cross-border program Italy-France Maritime 2007–2013.

Appendix 1

The parameters involved in the gust response factor in Eq. (10) can be derived in closed form.
The equivalent variance and period in Eq. (10) read [22]:

$$\mathscr{C}^2 = \frac{\gamma^{*20}\left(\frac{T_{\max}}{T_{tot}} - 1\right) + \Lambda^5 - \frac{5}{2}\Lambda^4\Phi + \frac{10}{3}\Lambda^3\Phi^2 - \frac{5}{2}\Lambda^2\Phi^3 + \Lambda\Phi^4 - \frac{1}{6}\Phi^5}{\gamma^{*16}\left(\frac{T_{\max}}{T_{tot}} - 1\right) + \Lambda^4 - 2\Lambda^3\Phi + 2\Lambda^2\Phi^2 - \Lambda\Phi^3 + \frac{1}{5}\Phi^4} \tag{41}$$

$$T_{eq} = \frac{\gamma^{*16}(T_{\max} - T_{tot}) + \widetilde{T}_{tot}\left(\Lambda^4 - 2\Lambda^3\Phi + 2\Lambda^2\Phi^2 - \Lambda\Phi^3 + \frac{1}{5}\Phi^4\right)}{\left[\mathscr{C}^2\right]^4} \tag{42}$$

with $T_{\max} = 600$s and

$$\begin{aligned} &T_{\text{tot}} = T_1 + T_N; \qquad T_1 = \frac{T}{2}; \qquad T_2 = T_1\left(1 + \frac{1}{2\xi T n_1}\right); \qquad T_N = \begin{cases} T_2, & T_2 \le T_{\max}/2 \\ T_{\max}/2, & \text{otherwise} \end{cases} \\ &\Lambda = \gamma^{*4} + \Phi; \qquad \Phi = \beta\left(1 + \gamma^{*4}\right); \qquad \beta = \frac{1}{1 + \frac{1}{4\xi T n_1}}. \end{aligned} \tag{43}$$

A closed-form solution is also available for the Davenport peak factor:

$$g_q = \sqrt{2\ln(\nu_q T_{eq})} + \frac{0.5772}{\sqrt{2\ln(\nu_q T_{eq})}} \tag{44}$$

with

$$\nu_q = n_1\sqrt{\frac{R^2}{B^2 + R^2}}. \tag{45}$$

The background and resonance factors in Eqs. (10) and (45) can be estimated in closed form as follows [15,83]

$$B^2 = \frac{1}{1 + 0.9\left[\frac{b(z_e)+H}{L_v(z_e)}\right]^{0.63}} \tag{46}$$

$$R^2 = \frac{\pi}{4\xi} S_{\dot{v}}(z_e, n_1)\eta_b\eta_H \tag{47}$$

where $z_e = 0.6H$ and

$$\eta_\varepsilon = \frac{4n_1\varepsilon(z_e)}{v_{\text{m}}\alpha(z_e)} \tag{48}$$

with $\varepsilon = b, H$.

Appendix 2

To investigate the influence of each uncertain parameter, this appendix presents the plots of EPSD obtained by setting a single uncertain parameter at its LB and UB while fixing the others at their midpoint. Fig. 22 and Fig. 23 plot the interval EPSD associated with the LB (Fig. 22a, Fig. 23a) and UB (Fig. 22b, Fig. 23b) of the parameters γ^{*I} and T^I, respectively.

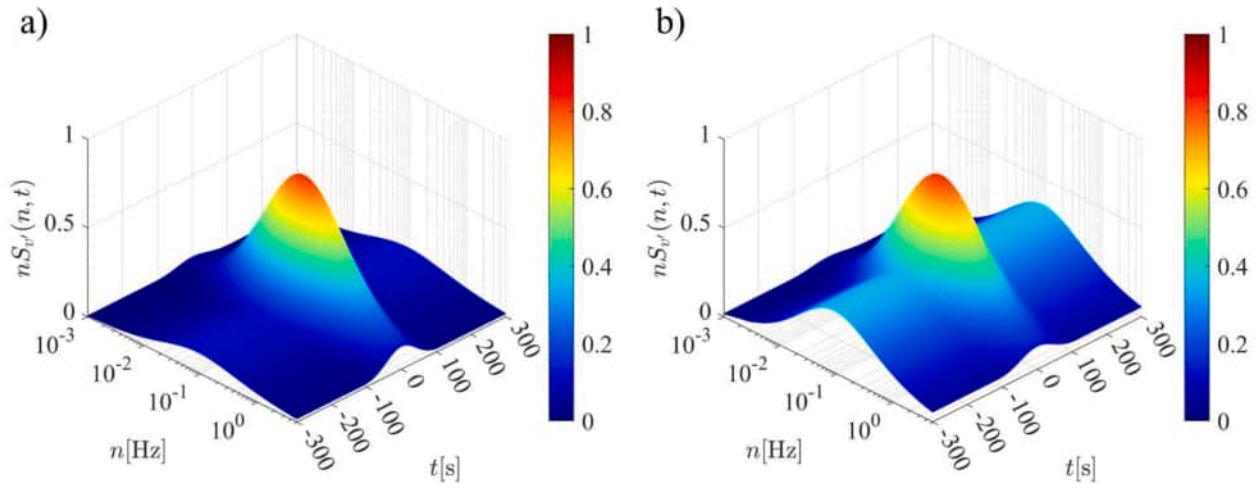

Fig. 22. Interval EPSD of the nonstationary turbulence v' evaluated for different values of the interval variables: (a) $\gamma^{*I} = \underline{\gamma}^*$, $T^I = T_0$, $z_m^I = z_{m,0}$, $I_v^I = I_{v,0}$, $L_v^I = L_{v,0}$; (b) $\gamma^{*I} = \overline{\gamma}^*$, $T^I = T_0$, $z_m^I = z_{m,0}$, $I_v^I = I_{v,0}$, $L_v^I = L_{v,0}$.

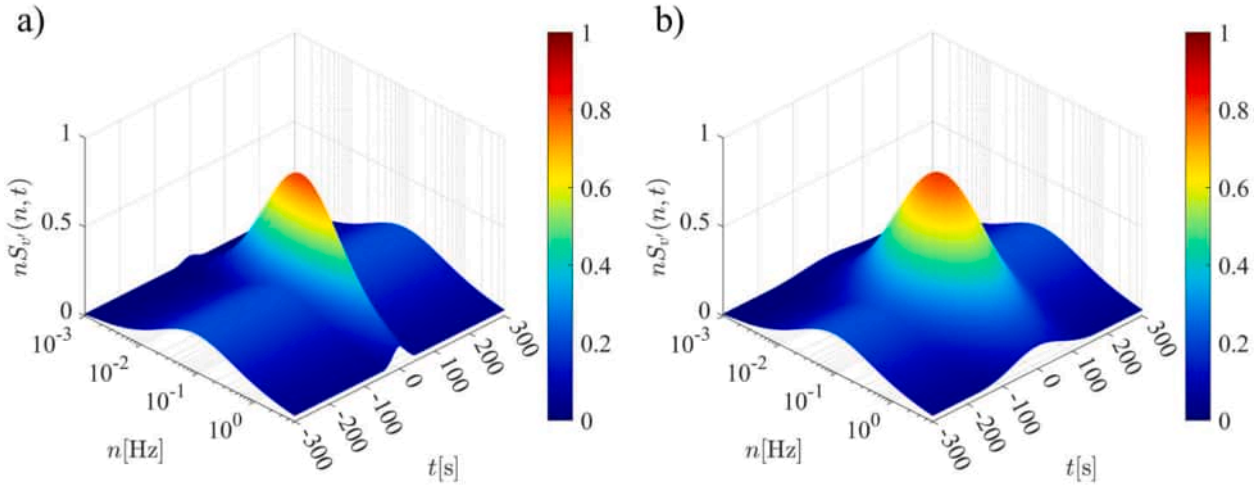

Fig. 23. Interval EPSD of the nonstationary turbulence v' evaluated for different values of the interval variables: (a) $T^I = \underline{T}$, $\gamma^{*I} = \gamma_0^*$, $z_m^I = z_{m,0}$, $I_v^I = I_{v,0}$, $L_v^I = L_{v,0}$; (b) $T^I = \overline{T}$, $\gamma^{*I} = \gamma_0^*$, $z_m^I = z_{m,0}$, $I_v^I = I_{v,0}$, $L_v^I = L_{v,0}$.

In agreement with Fig. 5, it is shown that the uncertainty on the parameter T^I in Fig. 23 affects the EPSD, especially in the neighbourhood of $t = 0$s. Instead, Fig. 22 shows that the uncertainty on the parameter γ^{*I} affects the EPSD significantly, causing a change in the height of the peak for $|t| > \frac{T^I}{2}$. It is worth noting, however, that the main peak of the interval EPSD is not affected by the uncertainties associated with the interval parameters γ^{*I} and T^I.

Fig. 24 and Fig. 25 plot the interval EPSD associated with the LB (Fig. 24a, Fig. 25a) and UB (Fig. 24b, Fig. 25b) of the parameters z_m^I and L_v^I, respectively.

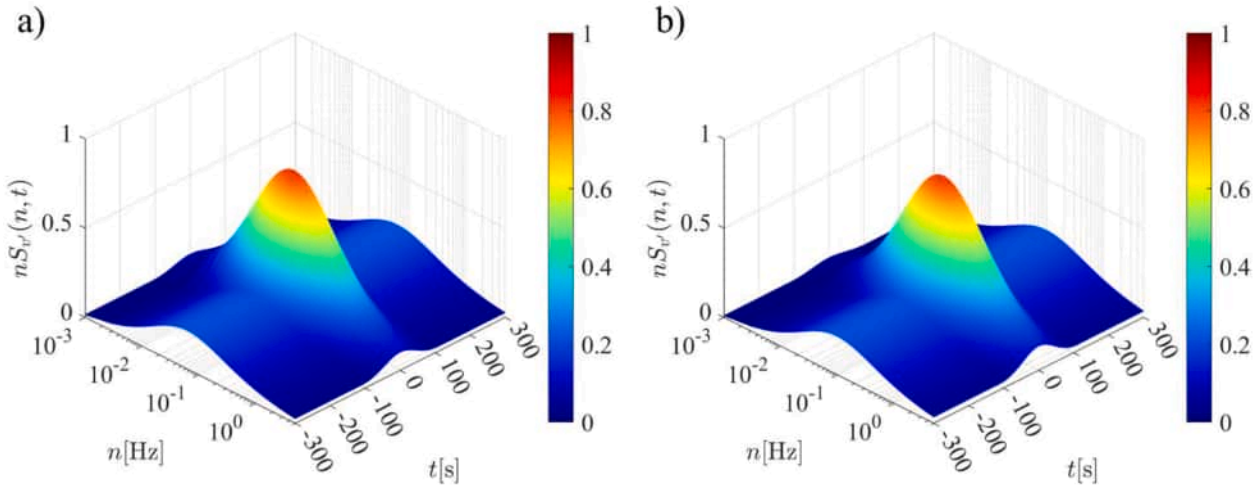

Fig. 24. Interval EPSD of the nonstationary turbulence v' evaluated for different values of the interval variables: (a) $z_m^I = \underline{z}_m$, $\gamma^{*I} = \gamma_0^*$, $T^I = T_0$, $I_v^I = I_{v,0}$, $L_v^I = L_{v,0}$; (b) $z_m^I = \overline{z}_m$, $\gamma^{*I} = \gamma_0^*$, $T^I = T_0$, $I_v^I = I_{v,0}$, $L_v^I = L_{v,0}$.

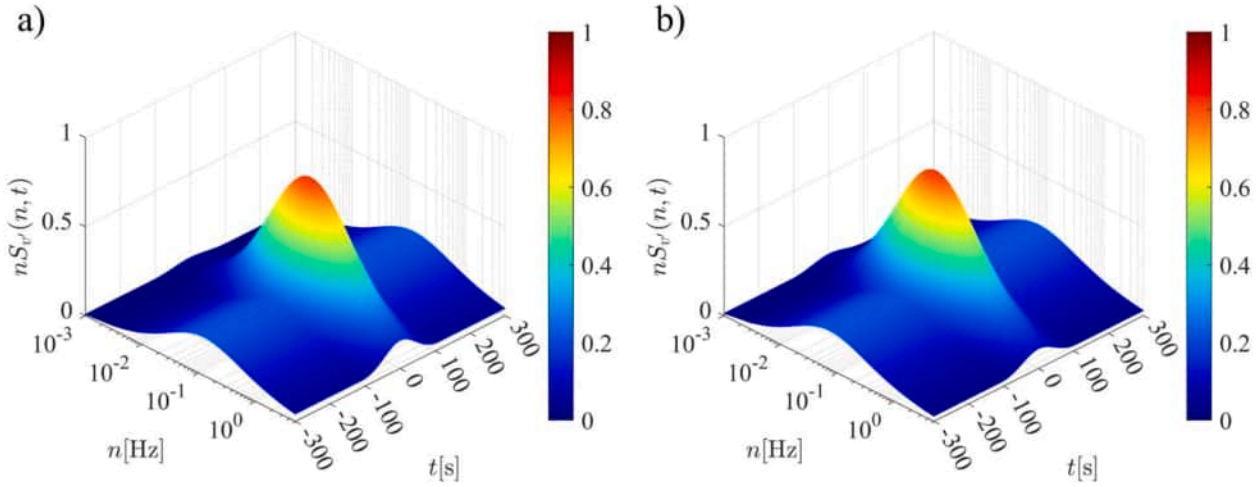

Fig. 25. Interval EPSD of the nonstationary turbulence v' evaluated for different values of the interval variables: (a) $L_v^I = \underline{L}_v$, $\gamma^{*I} = \gamma_0^*$, $T^I = T_0$, $z_m^I = z_{m,0}$, $I_v^I = I_{v,0}$; (b) $L_v^I = \overline{L}_v$, $\gamma^{*I} = \gamma_0^*$, $T^I = T_0$, $z_m^I = z_{m,0}$, $I_v^I = I_{v,0}$.

As observed in Fig. 7, the uncertainties associated with the parameters z_m^I and L_v^I affect the interval EPSD, shifting the peak towards higher or lower frequencies without changing its shape. As previously observed for the interval parameters γ^{*I} and T^I, also in these cases, the main peak of the interval EPSD is not affected by the uncertainties associated with z_m^I and L_v^I.

For the sake of completeness, Fig. 26 plots the interval EPSD associated with the LB (Fig. 26a) and UB (Fig. 26b) of the parameter I_v^I.

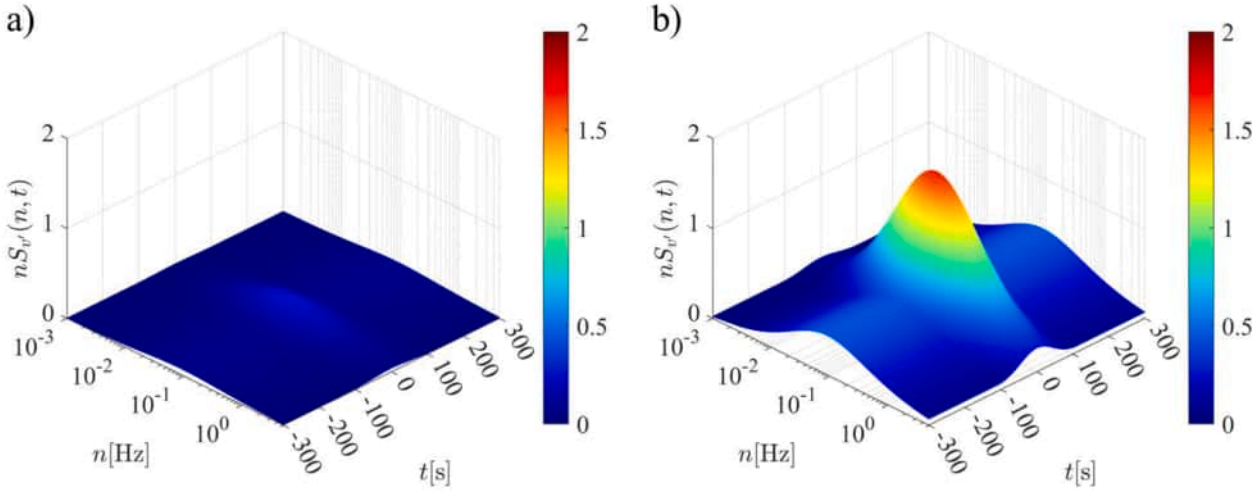

Fig. 26. Interval EPSD of the nonstationary turbulence v' evaluated for different values of the interval variables: (a) $I_v^I = \underline{I}_v$, $\gamma^{*I} = \gamma_0^*$, $T^I = T_0$, $z_m^I = z_{m,0}$, $L_v^I = L_{v,0}$; (b) $I_v^I = \overline{I}_v$, $\gamma^{*I} = \gamma_0^*$, $T^I = T_0$, $z_m^I = z_{m,0}$, $L_v^I = L_{v,0}$.

Differently from what is observed in Figs. 22–25, the uncertainties associated with the parameter I_v^I affect the interval EPSD exclusively in terms of magnitude, as can be easily inferred from Eq. (22).

Data availability

Data will be made available on request.

References

[1] Solari G. Thunderstorm downbursts and wind loading of structures: progress and prospect. Front Built Environ 2020;6.
[2] Solari G. Wind Science and engineering: origins, developments, fundamentals and advancements. Switzerland: Springer; 2019.
[3] Davenport AG. The application of statistical concepts to the wind loading of structures. ICE Proc 1961;19:449–72.
[4] Fujita TTheodore. The downburst: microburst and macroburst. Chicago: University of Chicago Press; 1985.
[5] Lombardo FT, Smith DA, Schroeder JL, Mehta KC. Thunderstorm characteristics of importance to wind engineering. J Wind Eng Ind Aerodyn 2014;125:121–32.
[6] Vicroy D. A simple, analytical, axisymmetric microburst model for downdraft estimation. NASA Tech Memo 1991.
[7] Li C, Li QS, Xiao YQ, Ou JP. A revised empirical model and CFD simulations for 3D axisymmetric steady-state flows of downbursts and impinging jets. J Wind Eng Ind Aerodyn 2012;102:48–60.
[8] Wood GS, Kwok KCS, Motteram NA, Fletcher DF. Physical and numerical modelling of thunderstorm downbursts. J Wind Eng Ind Aerodyn 2001;89:535–52.
[9] Wood GS, Kwok KCS. An empirically derived estimate for the mean velocity profile of a thunderstorm downburst. In: Proceedings of the 7th AWES workshop; 1998.
[10] Chen L, Letchford CW. A deterministic-stochastic hybrid model of downbursts and its impact on a cantilevered structure. Eng Struct 2004;26:619–29.
[11] Solari G, Burlando M, De Gaetano P, Repetto MP. Characteristics of thunderstorms relevant to the wind loading of structures. Wind Struct An Int J 2015;20:763–91.
[12] Roncallo L, Solari G. An evolutionary power spectral density model of thunderstorm outflows consistent with real-scale time-history records. J Wind Eng Ind Aerodyn 2020;203.
[13] Davenport AG. Gust loading factors. J Struct Div 1967;93:11–34.
[14] Solari G. Alongwind Response estimation: closed form solution. J Struct Div 1983; 108:225–44.
[15] Solari G. Gust buffeting .2. Dynamic alongwind response. J Struct Eng-ASCE 1993; 119:383–98.
[16] Zhou Y, Kareem A. Gust loading factor: new model. J Struct Eng (N Y N Y) 2001; 127:168–75.
[17] Kareem A, Hu L, Guo Y, Kwon D-K. Generalized wind loading chain: time-frequency modeling framework for nonstationary wind effects on structures. J Struct Eng (U S) 2019;145.
[18] Hu L, Xu YL. Extreme value of typhoon-induced non-stationary buffeting response of long-span bridges. Probabilistic Eng Mech 2014;36:19–27.
[19] Huang G, Chen X, Liao H, Li M. Predicting of tall building response to non-stationary winds using multiple wind speed samples, wind and structures. Int J 2013;17:227–44.
[20] Kwon DK, Kareem A. Towards codification of thunderstorm/downburst using gust front factor: model-based and data-driven perspectives. Eng Struct 2019;199: 109608.
[21] Roncallo L, Solari G, Muscolino G, Tubino F. Maximum dynamic response of linear elastic SDOF systems based on an evolutionary spectral model for thunderstorm outflows. J Wind Eng Ind Aerodyn 2022;224:104978.
[22] Roncallo L, Tubino F. Thunderstorm gust response factor: a closed-form solution. J Wind Eng Ind Aerodyn 2023;240:105487.
[23] Roncallo L, Gimondo M, Tubino F. Dynamic response of slender vertical structures subjected to thunderstorm outflows. Appl Sci 2023;13.
[24] Zhang S, Solari G, De Gaetano P, Burlando M, Repetto MP. A refined analysis of thunderstorm outflow characteristics relevant to the wind loading of structures. Probabilistic Eng Mech 2018.
[25] Roncallo L, Tubino F. Thunderstorm gust Response factor: general tendencies and sensitivity analysis. J Wind Eng Ind Aerodyn 2023;236:105376.
[26] Oberkampf WL, Helton JC, Sentz K. Mathematical representation of uncertainty. In: Proceedings of the 19th AIAA applied aerodynamics conference; 2001. p. 1–23.
[27] Der Kiureghian A, Ditlevsen O. Aleatory or epistemic? Does it matter? Struct Saf 2009;31:105–12.
[28] Moens D, Vandepitte D. A survey of non-probabilistic uncertainty treatment in finite element analysis. Comput Methods Appl Mech Eng 2005;194:1527–55.
[29] I. Elishakoff, M. Ohsaki, Optimization and anti-optimization of structures under uncertainty, (2010).
[30] Elishakoff I. Possible limitations of probabilistic methods in engineering. Appl Mech Rev 2000;53:19–36.
[31] Faes M, Moens D. Recent trends in the modeling and quantification of non-probabilistic uncertainty. Arch Comput Methods Eng 2020;27:633–71.
[32] Corotis RB. An overview of uncertainty concepts related to mechanical and civil engineering. ASCE-ASME J Risk Uncertain Eng Syst B: Mech Eng 2015;1:40801.
[33] Ben-Haim Y. A non-probabilistic concept of reliability. Struct Saf 1994;14:227–45.
[34] Moore RE. Interval analysis. Prentice-Hall; 1966.
[35] Moore RE, Kearfott RB, Cloud MJ. Introduction to interval analysis. Soc Ind Appl Math 2009.
[36] Ben-Haim Y, Elishakoff I. Convex models of uncertainty in applied mechanics. Amsterdam: Elsevier; 1990.
[37] Zadeh LA. Fuzzy sets. Inf Control 1965;8:338–53.
[38] Beer M, Zhang Y, Quek ST, Phoon KK. Reliability analysis with scarce information: comparing alternative approaches in a geotechnical engineering context. Struct Saf 2013;41:1–10.
[39] Jiang C, Bi RG, Lu GY, Han X. Structural reliability analysis using non-probabilistic convex model. Comput Methods Appl Mech Eng 2013;254:83–98.
[40] Sofi A, Muscolino G, Giunta F. A sensitivity-based approach for reliability analysis of randomly excited structures with interval axial stiffness. ASCE-ASME J Risk Uncertain Eng Syst B: Mech Eng 2020;6:41008.
[41] Valdebenito M, Beer M, Jensen H, Chen J, Wei P. Fuzzy failure probability estimation applying intervening variables. Struct Saf 2020;83:101909.
[42] Sofi A, Giunta F, Muscolino G. Reliability analysis of randomly excited FE modelled structures with interval mass and stiffness via sensitivity analysis. Mech Syst Signal Process 2022;163:107990.
[43] Zheng X, Yao W, Gong Z, Zhang X. Learnable quantile polynomial chaos expansion: an uncertainty quantification method for interval reliability analysis. Reliab Eng Syst Saf 2024;245:110036.
[44] Zhao H, Fu C, Zhang Y, Wan Z, Lu K. A non-probabilistic reliability-based design optimization method via dimensional decomposition-aided Chebyshev metamodel. Reliab Eng Syst Saf 2025;262:111208.
[45] Alibrandi U, Koh CG. First-order reliability method for structural reliability analysis in the presence of random and interval variables. J Risk Uncertain Eng Syst B: Mech Eng 2015;1:41006.
[46] Jiang C, Zheng J, Han X. Probability-interval hybrid uncertainty analysis for structures with both aleatory and epistemic uncertainties: a review. Struct Multidiscip Optim 2018;57:2485–502.
[47] Xiao T, Park C, Lin C, Ouyang L, Ma Y. Hybrid reliability analysis with incomplete interval data based on adaptive Kriging. Reliab Eng Syst Saf 2023;237.
[48] Ouyang L, Che Y, Park C, Chen Y. A novel active learning Gaussian process modeling-based method for time-dependent reliability analysis considering mixed variables. Reliab Eng Syst Saf 2024;244:109916.
[49] Dong S, Zhong A, Li L, Li H, Yuan T. Hybrid reliability analysis based on an active learning method considering the coupling effects of random-interval uncertainty. Reliab Eng Syst Saf 2026;265:111486.
[50] Yuan X, Faes M, Valdebenito M, Liu S, Beer M. Efficient imprecise reliability analysis using the augmented space integral. Reliab Eng Syst Saf 2021.
[51] Ling C, Yang L, Feng K, Kuo W. Survival signature based robust redundancy allocation under imprecise probability. Reliab Eng Syst Saf 2023;239:109510.
[52] Yang L, Zhang X, Lu Z, Fu Y, Moens D, Beer M. Reliability evaluation of a multi-state system with dependent components and imprecise parameters: a structural reliability treatment. Reliab Eng Syst Saf 2024;250.
[53] Muscolino G, Genovese F, Sofi A. Reliability bounds for structural systems subjected to a set of recorded accelerograms leading to imprecise seismic power spectrum. ASCE-ASME J Risk Uncertain Eng Syst A: Civ Eng 2022;8:4022009.
[54] Behrendt M, Bittner M, Comerford L, Beer M, Chen J. Relaxed power spectrum estimation from multiple data records utilising subjective probabilities. Mech Syst Signal Process 2022;165:108346.
[55] Bittner M, Behrendt M, Beer M. Relaxed evolutionary power spectral density functions: A probabilistic approach to model uncertainties of non-stationary stochastic signals. Mech Syst Signal Process 2024;211:111210.
[56] Behrendt M, Faes M, Valdebenito M, Beer M. Estimation of an imprecise power spectral density function with optimised bounds from scarce data for epistemic uncertainty quantification. Mech Syst Signal Process 2023;189:110072.
[57] Behrendt M, Dang C, Beer M. Data-driven and physics-based interval modelling of power spectral density functions from limited data. Mech Syst Signal Process 2024; 208:111078.
[58] Sofi A, Genovese F. Stochastic analysis of combined primary-secondary structures subjected to imprecise seismic excitation. Eng Struct 2025;322:118885.
[59] Muscolino G, Sofi A. Stochastic analysis of structures with uncertain-but-bounded parameters via improved interval analysis. Probabilistic Eng Mech 2012;28: 152–63.
[60] Chauvenet W. A Manual of Spherical and practical astronomy: theory and use of astronomical instruments, method of least squares. J. B. Lippincott & Company; 1863.
[61] Barbato G, Barini E, Genta G, Levi R. Features and performance of some outlier detection methods. J Appl Stat 2011;38:2133–49.
[62] Fina M, Lauff C, Faes M, Valdebenito M, Wagner W, Freitag S. Bounding imprecise failure probabilities in structural mechanics based on maximum standard deviation. Struct Saf 2023;101:102293.
[63] Roncallo L, Tubino F, Gimondo M. Alongwind dynamic response of slender vertical structures: thunderstorm outflows vs extra-tropical cyclones. J Phys Conf Ser, Inst Phys 2024:242003.
[64] Roncallo L, Mavromatis I, Kougioumtzoglou IA, Tubino F. Fractional-order filter approximations for efficient stochastic response determination of wind-excited linear structural systems. Probabilistic Eng Mech 2024:103696.

[65] Solari G, Piccardo G. Probabilistic 3-D turbulence modeling for gust buffeting of structures. Probabilistic Eng Mech 2001;16:73–86.
[66] Romanic D. Mean flow and turbulence characteristics of a nocturnal downburst recorded on a 213-m tall meteorological tower. J Atmos Sci 2021;78:3629–50.
[67] Tubino F, Pagnini LC, Piccardo G. Uncertainty propagation in the serviceability assessment of footbridges. Struct Infrastruct Eng 2020;16:123–37.
[68] Pagnini LC. Model reliability and propagation of frequency and damping uncertainties in the dynamic along-wind response of structures. J Wind Eng Ind Aerodyn 1996;59:211–31.
[69] Pagnini LC, Repetto MP. The role of parameter uncertainties in the damage prediction of the alongwind-induced fatigue. J Wind Eng Ind Aerodyn 2012; 104–106:227–38.
[70] Solari G, Repetto MP, Burlando M, De Gaetano P, Pizzo M, Tizzi M, Parodi M. The wind forecast for safety management of port areas. J. Wind Eng. Ind. Aerodyn. 2012;104–106:266–77.
[71] F. Canepa, M. Burlando, M.P. Repetto, Thunderstorm outflows in the Mediterranean Sea area, (2023). 10.5281/zenodo.7495116.
[72] Burlando M, Zhang S, Solari G. Monitoring, cataloguing, and weather scenarios of thunderstorm outflows in the northern Mediterranean. Nat Hazards Earth Syst Sci 2018;18:2309–30.
[73] Flay RGJ, Stevenson DC. Integral length scales in strong winds below 20 m. J Wind Eng Ind Aerodyn 1988;28:21–30.
[74] Crespo LG, Kenny SP, Giesy DP. Interval predictor models with a linear parameter dependency. J Verif Valid Uncertain Quantif 2016;1:21007.
[75] Imholz M, Faes M, Vandepitte D, Moens D. Robust uncertainty quantification in structural dynamics under scarse experimental modal data: a bayesian-interval approach. J Sound Vib 2020;467:114983.
[76] Elishakoff I, Sarlin N. Uncertainty quantification based on pillars of experiment, theory and computation. Part I: data analysis. Mech Syst Signal Process 2016;74: 29–53.
[77] Vicroy DD. Assessment of microburst models for downdraft estimation. J Aircr 1992;29:1043–8.
[78] Hjelmfelt MR. Structure and life cycle of microburst outflows observed in Colorado. J. Appl. Meteorol. 1988;27:900–27.
[79] Canepa F, Burlando M, Solari G. Vertical profile characteristics of thunderstorm outflows. J Wind Eng Ind Aerodyn 2020;206.
[80] Solari G, Rainisio D, De Gaetano P. Hybrid simulation of thunderstorm outflows and wind-excited response of structures. Meccanica 2017;52:3197–220.
[81] Mason MS, Yanga T, George T, Paxton O, Wong E. An experimental investigation of the unsteady pressures on square cylinders in a non-stationary wind field. In: Proceedings of the 8th international colloquium. On bluff-body aerodynamics and applications; 2016.
[82] Yang T, Mason MS. Aerodynamic characteristics of rectangular cylinders in steady and accelerating wind flow. J Fluids Struct 2019;90:246–62.
[83] Solari G. Equivalent wind spectrum technique: theory and applications. J Struct Eng-ASCE 1988;114:1303–23.